Accepted Manuscript

Shear angle and amount of extension calculations for normal faults emanating from a detachment: Implications on mechanisms to generate rollovers

Hodei Uzkeda, Josep Poblet, Mayte Bulnes

PII: S0191-8141(14)00145-X

DOI: 10.1016/j.jsg.2014.07.006

Reference: SG 3093

To appear in: *Journal of Structural Geology*

Received Date: 5 March 2013

Revised Date: 2 July 2014

Accepted Date: 10 July 2014

SHEAR ANGLE AND AMOUNT OF EXTENSION CALCULATIONS FOR NORMAL FAULTS EMANATING FROM A DETACHMENT: IMPLICATIONS ON MECHANISMS TO GENERATE ROLLOVERS

UZKEDA, Hodei[1]*; POBLET, Josep[1]; BULNES, Mayte[1]

[1]: Departamento de Geología, Universidad de Oviedo, C/Jesús Arias de Velasco s/n, 33005 Oviedo, Spain. E-mail (Uzkeda): hodei@geol.uniovi.es, e-mail (Poblet): jpoblet@geol.uniovi.es, e-mail (Bulnes): maite@geol.uniovi.es

*: Corresponding author. Tel: +34 98 5103120. Fax: +34 98 5103103. Now at Royal Holloway University of London.

KEYWORDS

Vertical/inclined shear; extension; normal fault; detachment; rollover.

ABSTRACT

The reconstruction/restoration/modelling of normal faults (both listric and planar) emanating from a detachment at depth and their associated rollover folds, using the vertical or inclined shear method is widely utilized because its simplicity and the information it can provide. However, it has a rather serious issue derived from the uncertainty about the shear angle, the type of shear and the amount of extension that should be employed in each situation. Here we describe a new methodology that, using easily acquired input data, allows estimation of whether the shear was vertical, antithetic or synthetic and the values for both the shear dip and the amount of extension. These calculations rely on the use of graphs of throw versus heave for different horizons affected by the normal fault and the associated rollover, and are checked using an area-based method which permits the determination of whether these values are correct. These graphs may be used as a predictive tool or as a guide to show how the assumptions deviate, such as distinguishing quickly whether other mechanisms apart from vertical/inclined shear took place. The effects of syn-extension sedimentation and reverse fault reactivation on the proposed method are also examined. The analysis of experimental and natural examples shows that the initiation of some rollovers with a component of fault-propagation and/or drag folding, and/or development of a crestal collapse graben cause the estimated shear dips to be smaller than the actual values and the amounts of extension to be greater. In addition, these analyses show that the shear dip may increase with increasing extension.

1. Introduction

Normal faults emanating from detachments at depth are a type of structure widely represented in nature and, consequently, the subject of multiple studies. Many of these analyses are focused on developing techniques to reconstruct the faults and/or their associated rollover folds from the available data. Diverse methods to calculate the depth of the detachment from which the fault would emanate have been developed: a) those based on the lost area rule (adaptation of the Chamberlin (1910) method for normal faults); b) those that rely on the rotation of rigid blocks along circular faults (Moretti et al., 1988); c) lost-area diagrams (Groshong, 1994, 1996); and d) graphs of best linear fit of detachment depths (Bulnes and Poblet, 1999) adapted to normal faults. There are also techniques allowing the determination of the complete shape of the fault at depth, such as: a) those based on vertical shear, known as the chevron construction or constant heave (Verrall, 1981), or on inclined shear both synthetic and antithetic (White et al., 1986; Dula, 1991), including subsidiary faults (Song and Cawood, 2001), with layer-parallel strain (Groshong, 1990) or with fault parallel shear (Williams and Vann, 1987); b) those considering constant displacement along the fault (Williams and Vann, 1987); and c) constructions founded on flexural slip (Davison, 1986) or constant thickness beds (Morris and Ferrill, 1999) (Figure 1). Most of these methods permit also to model the rollover resulting from the fault activity. This construction is also feasible from other techniques such as: a) the one for circular faults and rigid blocks (Moretti et al., 1988), b) models based on fault-bend folds (Groshong, 1989; Xiao and Suppe, 1992), c) finite difference assuming uncompressible flow (Waltham, 1989), and d) hangingwall collapse following the Coulomb criteria comparable to simple shear (Tearpock and Bischke, 1991). The experimental models generated in the laboratory have also substantially helped the understanding of normal faults because they allow assessment of parameters such as amount of extension, fault shape, etc. (McClay and Ellis, 1987a, 1987b; Ellis and McClay, 1988; McClay, 1989, 1990a, 1990b, 1995, 1996; Schlische et al., 2002 and Henza et al., 2010 amongst others). One of the main issues derived from the plethora of available procedures is that the resulting reconstructions obtained may vary enormously depending on the technique employed (Figure 1). Thus, the selection of one or another method is of great importance.

The methods based on vertical/inclined shear are the most utilized. Despite the simplification they imply about the particle motion, they make predictions on the fault shape and detachment depth (e.g., Verrall, 1981; White et al., 1986), the rollover morphology (e.g., Matos, 1993), the algorithms to forward model and/or restore the structures and the deformation undergone (e.g., Matos, 1993; Poblet and Bulnes, 2007) easily. Furthermore, they have been proved to be suitable methods for modelling both natural (Groshong, 1990; White and Yielding, 1991; Matos, 1993; Poblet and Bulnes, 2005a) and experimental examples (Groshong, 1990; Poblet and Bulnes, 2005a, 2005b). Consequently, the vertical/inclined shear methods are considered to be a good approximation of the behaviour of the hangingwall of normal faults during extension (McClay et al., 1995). However, the uncertainty about the type of shear and the shear angle that should be chosen in each case constitutes a crucial disadvantage for their application, as different angles result in dissimilar results (Figures 1c, 1d and 1e). There are diverse approaches to estimate the shear angle and its character (synthetic, vertical or antithetic): a) shear parallel to the rollover axial traces (Xiao and Suppe, 1992), b) shear parallel to the subsidiary faults associated with the main one (White et al., 1986; Xiao and Suppe, 1992), c) the trial and error method (White and Yielding, 1991), and d) quantitative methods that require knowing the amount of layer-parallel strain and the rollover general dip (Groshong, 1990).

The horizontal extension is another parameter that controls greatly the results. Some of the methods to estimate it from the available data were proposed originally for contraction, but were adapted to extensional settings: a) comparison between unfolded bed length and structure width (Gwinn, 1970), b) maximum displacement along the fault (Chapman and Williams, 1984), c) fault heave (Ziegler, 1982; Jackson and Galloway, 1984; Barr, 1985), d) mean between the extension estimated using bed length and the maximum fault displacement (Williams and Vann, 1987), e) rollover axial traces separation (Xiao and Suppe, 1992), and f) slope of the lost-area best-fit function (Groshong, 1994, 1996). Dissimilar extension values are obtained depending on the technique employed (Poblet and Bulnes, 2005a, 2005b), which has important consequences for the predictions that can be made.

We present a new method that provides estimation of the shear properties (dip and character) and of the amount of extension to model normal faults. The main difference with previous procedures is that it is able to estimate both parameters using simply a portion of the main fault offsetting a minimum of, at least theoretically, two horizons, although to use more horizons is recommended. The method only requires simple measurements on a geological section across a fault, projecting them on a graph and finding a best-fit function for the plotted data. Theoretically, this method could be used as a predictive tool. However, its application to experimental and natural examples suggests that it supplies minimum shear dips and maximum amounts of extension that get closer to actual values for faults with high amounts of extension. Checking the results using a new area-based method, which involves comparison between the area in the present-day, deformed section, and that in an undeformed section, supports this conclusion. In addition, the method presented can help in determining how much studied structures deviate from the expected behaviour if they were solely the result of vertical/inclined shear with a uniform dip.

2. Analysis of the heave, throw and displacement in normal faults with associated rollovers

One of the aims of this work is to find a procedure that allows the determination of: 1) the shear dip, 2) the shear character (antithetic, vertical or synthetic) and 3) the amount of extension taking as input parameters the heave, throw and displacement of several horizons along a fault. This makes of capital importance a thorough analysis of how the fault slip components vary along successions offset by normal faults emanating from a detachment. In any normal fault the horizon located at the detachment level has a null throw, which implies that the heave and the displacement are the same and, assuming no strain within the hangingwall, equal to the extension. To visualize how these parameters vary for the rest of the horizons, theoretical rollover were created using the models of vertical shear (Verrall, 1981), inclined shear (White et al, 1986), flexural slip (Davison, 1986) and constant thickness beds (Morris and Ferrill, 1999). They were built using different values of extension and fault shapes (ramp-flat, segmented, cubic or arctangent functions, splines) (Figure 2). The models created are based on a series of assumptions: a) the hangingwall is deformed as a rollover (fault-bend folding) according to the inclined or vertical shear mechanisms and combinations of mechanisms are not considered, b) the shear dip is constant over time and all along the whole hangingwall, c) the geometry of the fault and the footwall beds does not vary along the process, and d) compaction is not considered. In this paper we present only the most significant cases analyzed. For each geological section we measured the heave, throw, displacement, and stratigraphic height with respect to an arbitrary reference level of the horizons offset by the fault (Figure 3a). Subsequently, we plotted the fault slips of each horizon versus its stratigraphic height on one graph (Figure 3b), and its throw versus its heave on another graph (Figure 3c). The later graphs are the foundation of the proposed methodology as it is more extensively explained in a section below.

The simplest case is a planar fault formed by a flat and a constant dip ramp. The values of heave, throw and displacement for the different horizons, plotted against their stratigraphic height, are constant for the horizons whose hangingwall cut-off points lay on the ramp (upper graphs in figure 4). The situation changes for those horizons whose cut-off points lay directly on the detachment. Irrespective of the type of shear and shear dip, displacement and throw always decrease stratigraphically downwards, whereas the behaviour of the heave depends on the shear angle applied to generate the rollover. With vertical shear (Figure 4a) the heave is constant along the whole stratigraphic succession; antithetic shear (Figure 4b) implies an increase of heave when moving towards deeper stratigraphic horizons; and synthetic shear (Figure 4c) shows a decrease of heave values stratigraphically downwards. In the throw versus heave graphs the points of horizons whose cut-offs are located on the ramp are superposed, since they all share the same values for heave and throw (lower graphs in figure 4). On the contrary, the points representing the horizons whose cut-off points lay on the detachment follow a straight line that may be vertical (vertical shear) or inclined (antithetic and synthetic shear). The throw decreases as heave increases with antithetic shear (Figure 4b), whereas increments of throw imply increases of heave with synthetic shear (Figure 4c).

Similar graphs were generated for faults with more complex geometries. For example, we used listric faults built with the arctangent function (Figure 5). Throw and displacement diminish towards deeper stratigraphic levels in rollover constructed by vertical shear (upper graph in figure 5a). They show a continuous, smooth variation, which seems to depend on the fault geometry. Though, the general tendency (i.e. stratigraphically downwards decrease) is the same as in the ramp-flat fault. The heave has the same value for each and every horizon that is equal to the extension. It is smaller than displacement until reaching the detachment horizon where they are equal and throw is zero. The points representing the heave are located along the following function:

$$x = e \qquad (1),$$

where e is the extension. In addition, the curve depicting the displacement along the fault tends to be asymptotic to the straight line that fits the heave data in the horizons close to the detachment. Irrespective of the fault shape and amount of extension, the graphs of throw versus heave (lower graphs in figures 4a and 5a) are virtually identical (all the horizons have the same heave). This means that all the points are situated along a vertical straight line that responds to Eq. (1).

For rollover folds constructed using inclined shear and the same fault shape as above, the functions of throw and displacement versus their stratigraphic height (upper graphs in figures 5b and 5c) are analogous to those of vertical shear. Both the displacement and the throw decrease towards the detachment. Nevertheless, contrary to what happened with vertical shear, the heave varies along the stratigraphic succession and its variation allows us to recognise whether the shear is antithetic or synthetic and its dip. Antithetic shears imply a heave increment stratigraphically downwards (upper graph in figure 5b), whereas synthetic shears mean a heave decreasing down section (upper graph in figure 5c). The inclination of the best-fit line for the heave data depends on the shear dip. Shear dips close to 90º will be reflected in almost vertical straight lines, whereas gentler shear dip values will result in functions of greater curvatures and lesser slopes. As with the vertical shear, the displacement and heave curves tend to be asymptotic when approaching the detachment. In the graphs of throw versus heave (lower graphs in figures 5b and 5c) the points representing the different horizons may be fitted by the following linear function:

$$y = m \cdot x + n, \qquad (2)$$

where m:

$$m = tan(\alpha) \qquad (3),$$

α being the shear angle measured respect to the horizontal (i.e., the shear dip), and $m <$ 0 for antithetic shears (lower graph in figure 5b) and $m > 0$ for synthetic ones (lower graph in figure 5c). The intersection with the abscissae axis:

$$x = -n/m \qquad (4),$$

is the value of the extension, equal to the displacement of the horizon along the detachment. The explanation of this relation is shown in figure 6. In the case of antithetic shear, the larger the throw the smaller the heave (Figure 6a), because

$$h = e - t \cdot tan(\alpha) \qquad (5),$$

where h is the heave, e is the extension, α is the shear dip and t is the throw. In synthetic shear (Figure 6b) greater throws lead to larger heaves,

$$h = e + t \cdot tan(\alpha) \qquad (6).$$

The parameter that relates both values is the shear dip. From the expressions above we can deduce that the heave equals the extension when the throw is zero, i.e. at the detachment.

The method presented in the next section is not thought to be applied to rollovers built by flexural slip, in which bed thickness and lengths are maintained. Nevertheless, the analysis of the resulting graphs for these types of folds is interesting due to the information they may supply. We elaborated models of rollovers developed over listric normal faults formed by segments of constant dip following the method of Morris and Ferrill (1999) and others using the method of Davison (1986). In the graphs derived from the analysis of Morris and Ferrill (1999) structures, both the displacement along the fault and the throw tend to diminish when descending in the stratigraphic succession (upper graph in figure 7a). This variation is not continuous but shows steps as result of the segmented fault geometry. The heave behaves differently; it does not show a consistent trajectory, because, at least in the examples built, it increases downwards in the upper part of the stratigraphic succession and decreases downwards, broadly, in the lower one (upper graph in figure 7a). The behaviour of the throw versus heave function in the folds constructed using the Morris and Ferrill (1999) method would be equivalent to a variation in the shear character along the stratigraphic succession (lower graph in figure 7a), being comparable to antithetic (upper part of the graph) and synthetic (lower part). In the graphs obtained for the structures constructed following the method of Davison (1986), both the throw and displacement tend to decrease when moving down through the stratigraphic succession (upper graph in figure 7b). The heave takes values approximately constant in the upper part of the stratigraphic succession, but downwards it diminishes initially to grow at deeper levels. The throw versus heave function (lower graph in figure 7b) shows three different regions, an upper one in which heave is more or less invariable (as if vertical shear acted), a middle one where it decreases downwards (comparable to synthetic shear) and a lower one in which it increases downwards (as when antithetic shear acts).

3. Shear and extension determination via graphs and checking through area balancing

In the graphs of slip versus stratigraphic height we could not find a universal best-fit function which allowed, from the available data, to extrapolate the function and obtain parameters as, for instance, the detachment depth. However, the evolution of the heave permits to recognize if vertical or inclined shear has acted, giving, in addition, qualitative information on the shear dip (the smaller the slope of the heave function the gentler the shear dip) and its synthetic or antithetic character (heave decreases down section with synthetic shear and increases with antithetic shear). These graphs may also help to find out whether the main mechanism responsible for the structure formation is different from vertical or inclined shear. In listric normal faults, if vertical or inclined shear acted the throw should decrease down section, together with the displacement (except for the horizons close to the detachment in which they may be constant or even increase slightly). Heave may increase, be constant or decrease (only one of the three options along the whole stratigraphic sequence) (Figure 5). Conversely, in ramp-flat normal faults the three parameters should remain constant except for the horizons lying directly on the detachment (Figure 4). If these premises are not met it is probable that a different mechanism has acted, alone or in conjunction with vertical/inclined shear. Despite that a graph derived from field, subsurface or experimental data exhibits similar characteristics to those described above, it does not ensure that vertical or inclined shear has really acted, as other mechanisms may provide similar results, at least along certain portions of the stratigraphic succession (upper graph of figure 7a).

Throw versus heave graphs do offer quantitative information. The arctangent of the slope of the best-fit linear function would be the shear dip, indicating also its vertical (infinite slope), antithetic (negative slope) or synthetic (positive slope) character (Figure 8). The amount of extension would be the intersection between the function and the x-axis (Figure 8), i.e. the heave value when the throw is zero. Once this information has been obtained, well-known techniques mentioned in the introduction section may be employed to reconstruct the geometry of the fault at depth from the rollover, or vice versa, to calculate the detachment depth, to choose the best restoration and/or forward modelling algorithm, and/or to estimate the strain.

The application of this procedure to rollover folds formed by mechanisms different from vertical or inclined shear will result in graphs of throw versus heave that cannot be fitted adequately by a linear function. In such case the structure should not be modelled employing vertical or inclined shear solely and a different mechanism or combinations of mechanisms must be invoked to explain its origin.

For those examples of structures in which the full geometry of the fault is available, the results can be checked using an area-based test that assumes plane strain. This procedure we propose consists of overlapping the present-day, deformed section (Figure 9a), on top of a theoretical, perfect undeformed section (Figure 9b) in such a way that the horizontal distance between the fault in the deformed section and that in the undeformed section is the extension value estimated (Figures 9c, 9d, 9e and 9f). This allows to recognize: 1) an approximately triangular region in the upper part of the overlapped sections (in dark grey in figures 9c, 9d, 9e and 9f) and 2) another region in the lower part of the overlapped sections (in light grey in figures 9c, 9d, 9e and 9f). If the area of these two regions is identical (Figure 9e), the application of the estimated shear to the undeformed horizons would lead to the formation of the rollover observed in the present-day, deformed section. This means that the values of shear dip and extension, estimated using the method proposed in this paper, are correct. That the area of the upper region is smaller than the area of the lower region (Figure 9f), would imply that the shear type deduced is correct but the estimated dip is less than the actual one and the estimated extension exceeds the actual one. In this case, a forward model of a rollover fold using the calculated values and the undeformed section as input data would not correctly simulate the structure in the present-day section. When the area of the upper, triangular region is greater than the area of the lower region, it means that the estimated parameters are not correct either (Figures 9c and 9d). This phenomenon occurs when the shear type deduced is incorrect or when it is correct but the estimated dip is larger than the actual value and the amount of extension is less than the actual one. As before, a forward model created with these values would not reproduce correctly the deformed section. The larger the difference between the area of the upper, triangular zone and that of the lower zone, the more erroneous the shear dip and extension values estimated. The implementation of this area-based verification method may allow to determine whether the values obtained using the slips-based method proposed in this paper are correct, and to constrain to some extent the range of correct values of shear dip and extension usually influenced by the erratic behaviour of the slips functions obtained.

4. Effects of tectonic inversion

The simplest case is when a normal fault developed by vertical or inclined shear is reactivated with a reverse sense of movement and with the same shear angle as that employed in the extensional event. In this case, the resulting graphs should be equal in shape to those obtained for normal faults without reverse reactivation (Figures 4 and 5). The reason is that the extensional process is partially, or totally, reverted. If the inversion is partial, the graphs allow to calculate the shear dip and the remnant extension after the contraction. If, on the contrary, the contraction exceeds the extension, so that horizons exhibit reverse fault displacements (Figure 10), the throw versus heave graph would be slightly different. The shear dip will still be the arctangent of the slope of the function, but now there will be no horizon with throw equal to zero (lower graph in figure 10a). However, the intersection of the best-fit function with the x-axis represents the value of the net contraction, i.e. difference between contraction and previous extension (about 5.60 units in the case of the example in figure 10a). These graphs are equal to those derived from fault-bend folds developed over thrusts or reverse faults in a purely compressive setting constructed using vertical/inclined shear. In the graphs of slips versus stratigraphic height the heave increases stratigraphically downwards, whereas the throw and the displacement diminish (upper graph in figure 10a).

Another option is that the reactivation is produced by vertical or inclined shear but with a shear dip different to that of the extension. The resulting graphs for a total inversion situation (Figure 10b) show a more erratic behaviour than those discussed above. For example, the throw does not decrease consistently along the stratigraphic sequence but it increases its value in some zones and diminishes in others. In the graph of throw versus heave the points are not aligned, as would be expected if the shear dip had remained constant during extension and contraction. This prevents the use of the method proposed here for such situations.

The graphs in figure 10c correspond to an extensional rollover formed according to the method of Davison (1986) developed on a normal fault subsequently reactivated using inclined shear until reaching total inversion. As expected, these graphs do not permit any estimation about the shear during the contraction or the amount of contraction because of the complex functions obtained.

5. Effects of syntectonic sedimentation

To check the possible incidences caused by sedimentation simultaneous to the fault activity we created two models, a growth normal fault with sedimentation during extension including pre-extension and syn-extension beds (Figure 11) and a growth normal fault with partial inversion in which pre-extension, syn-extension, post-extension pre-inversion, and syn-inversion beds were included (Figure 12).

In the fault slips versus stratigraphic height graph constructed for the growth normal fault (Figure 11a) two different tectono-stratigraphic units can be identified. The parameters of the lower unit, which corresponds to the pre-extension horizons, show the typical trajectory described above for rollover folds constructed with antithetic shear. On the contrary, the fault slips for the syn-extension horizons decrease stratigraphically upwards towards the top of the succession. The same tectono-stratigraphic units can be individualized in the throw versus heave graph (Figure 11b). The points corresponding to the pre-extension horizons follow a straight line whose slope indicates the shear dip used to create the rollover fold. In contrast, the syn-extension horizons do not exhibit a rectilinear trajectory, but they follow a curve. These horizons are not useful to determine the shear or the amount of extension using the method presented here. Thus, we conclude that any estimation should be exclusively performed using the pre-extension horizons.

In figure 12 a model of a growth normal fault, with subsequent inversion and the same shear dip and dip sense for both the extensional and contractional events, has been analyzed. The reverse slips in the graphs in figure 12 have been depicted as negative. In the slip versus stratigraphic height graph (Figure 12a) four different zones may be identified and used to separate four tectono-stratigraphic units. The pre-extension horizons exhibit the behaviour previously observed (Figures 4 and 5) when no syntectonic sedimentation occurred. In a graph of throw versus heave for only the pre-extension horizons (Figure 12c) we can calculate the shear dip, its character and the remnant extension after the inversion (intersection of the best-fit function with the x-axis). The boundary between the pre-extension and the syn-extension beds would correspond to the point that displays the greatest normal displacement along the fault (Figure 12a), or that after which the points of the throw versus heave graph (Figure 12b) depart from a rectilinear trajectory. Stratigraphically below the null point, the situation is the same as one can expect in a growth normal fault (Figure 11). The points in the throw versus heave graph representing the syn-extension horizons cannot be fit by a linear function since they show a curvilinear trajectory (Figure 12b). These horizons are useful for calculating neither the shear dip nor the amount of extension. These beds are overlain by layers deposited during a period of tectonic quiescence after the extension and prior to the inversion event. The absolute value of heave decreases stratigraphically upwards within these horizons, whereas the absolute values of throw and displacement increase (Figure 12a). In a throw versus heave graph for these horizons the points fall onto a straight line whose slope supplies information about the shear dip and its character (Figure 12d). The intersection between this function and the x-axis would indicate the amount of contraction (negative value). In the upper part of the stratigraphic sequence, the syn-inversion beds show a progressive loss of displacement, becoming null for the horizon deposited at present-day (Figures 12a and 12b). The points representing these horizons in the graphs seem to follow a straight line, however, this is probably because they have been transported along a constant dip segment of the fault. These syn-tectonic horizons should not be employed to calculate the shear angle, its character or the amount of contraction using the methodology described here.

According to the results obtained from figure 10b, if the contraction were produced through vertical or inclined shear whose dip were different to that of the shear during the extensional event, only data for the compressive stage (shear dip and character and amount of contraction) could be obtained utilizing the post-extension pre-inversion horizons.

6. Application to experimental and natural examples

The possible applicability of the method proposed in this study has been tested using experimental and natural examples of listric normal faults. We have chosen sequential physical experiments in order to compare the results obtained to different temporal stages of development of the same structure.

The first example corresponds to a clay experiment presented in Dula (1991). We used two sections constructed by the author (Figures 13a and 13d) derived from two photographs of different stages of the experiment (Figures 5d and 7a of Dula, 1991). In the graph of slips versus stratigraphic height obtained for the less extension stage (Figure 13a) the throw decreases slightly with depth, whereas the heave and the displacement tend to grow slowly with depth (Figure 13b). The fact that the increase in the displacement is slightly greater in the stratigraphically lowest horizon (this horizon practically rests on the detachment) might be indicative of antithetic shear according to the theoretical models studied above. According to the linear best-fit of the throw versus heave data (Figure 13c) the shear obtained is antithetic and dips 25º, notably smaller than that proposed by Dula (1991) estimated using the particle paths, whereas the extension is larger than the actual one (3.9 centimetres versus 2 centimetres). The extension calculated by Poblet and Bulnes (2005a) for this stage of the experiment using the shear angle suggested by Dula (1991) on different horizons ranges from 1.6 to 2.3 centimetres. The application of the area method presented above to this stage of the experiment also indicates that the estimated shear dip is substantially less than the correct one and that the estimated extension is larger than the actual one (Figure 14a). As a consequence, the model generated with these parameters fails to reproduce correctly the original shape of the clay experiment (Figure 13a). In the graph of slip versus stratigraphic height for the experimental stage with greater extension (Figure 13d) the displacement along the fault is pretty constant, whereas the heave grows with depth and the throw diminishes in a pronounced manner (Figure 13e). The constant displacement is apparently consistent with the theoretical models in which the horizons lying close to the detachment exhibit constant displacements when vertical or steeply dipping shear operates (Figures 4 and 5). The linear fit of the points depicted on the throw versus heave graph (Figure 13f) indicates an antithetic shear dipping slightly more than 63º. From the analysis of the displacement paths of material points, Dula (1991) determined an antithetic shear with a dip of 70º, somewhat large than that calculated employing our method. The intersection of the linear best-fit function with the x-axis yields an extension of 6.6 centimetres, slightly greater than the actual one (6 centimetres). Poblet and Bulnes (2005a) calculated the amount of extension for the same experiment employing the shear angle suggested by Dula (1991) on different horizons and their results varied from 6.2 to 8.0 centimetres, also larger than the actual one. The application of the area-based procedure described above to this stage of the experiment reinforces the observation that the estimated shear dip is somewhat less than the correct one and that the estimated extension is slightly larger than the actual one (Figure 14b). Thus, the rollover modelled with the calculated parameters is comparable to a certain extent to that of the clay experiment (Figure 13d). We conclude that the method proposed supplies better results for the last stage of the experiment than for the early stage, and that the shear dip is greater for the last stage than for the early stage.

The second example is a sequence of cross sections derived from photographs showing the evolution of a sand experiment run by Burger (2012) (Figure 15a). The slip versus stratigraphic height graphs (Figure 15b) show that the displacement is approximately constant along the stratigraphic succession in the last stages, whereas the heave tends to increase and the throw tends to decrease stratigraphically downwards. The linear best-fit functions for the throw versus heave data offer better extension values and shear dips for the last five stages (Figure 15c). As a consequence, the general geometry of the rollover folds modelled with the estimated parameters is not far from that of the experimental folds, overlooking the minor faults the inclined shear model is not able to predict (Figure 15d). One of the main discrepancies would be the tendency of the theoretical model to generate slightly wider half-grabens than the experimental ones in the early stages. The graphs of slip versus stratigraphic height (Figure 15b) point out that our method could not produce good results for the initial stages of the experiment. The slips show erratic behaviours for the first stages, growing and shrinking a number of times along the stratigraphic succession. In addition, the R-squared parameter for the best-fit functions in the throw versus heave graphs for the early stages of the experiment is very low (Figure 15c). In the more evolved stages, the deduced shear is antithetic and dips about 50º, with a faint tendency to increase in the last stages (from 48º to 53º dip). We compared the amounts of extension measured in the experiment with those estimated using the graphs for the last stages. We took as reference, assigning it an extension value equal to zero, the third stage of the evolution (the earliest one with a proper linear fit) (Figure 15e). The differences between both datasets are small, with discrepancies oscillating between 1% and 13% of the total extension. The application of the area method described above to the Burger (2012) experiment suggests that the estimated shear dip is less than the correct one and that the estimated extension is larger than the actual one, these differences being greater for the early stages than for the last stages, similarly to the Dula (1991) experiment.

The third example employed consists of a series of cross sections derived from photographs of different stages of a sand experiment carried out by Edwards (2013) (Figure 16a). In the slips versus stratigraphic height graphs constructed for the different stages of the experiment (Figure 16b), the heave increases stratigraphically downwards, the displacement is approximately constant, and the throw decreases down section. Although the path of the heave function is very similar to that obtained in faults formed by antithetic shear, the displacement does not exhibit an asymptotic trajectory and the heave does not decrease down section as in theoretical models (Figures 4 and 5). The value of the R-squared parameter points out that the throw versus heave data exhibits a slightly worse linear best-fit for the early stages of the experiment than for the late ones (Figure 16c). The extension obtained for each stage of the experiment (Figure 16c) reaches a maximum value of almost 7 cm. The values of extension obtained are between 0.72 and 1.04 cm higher than the actual values. The estimated shear is antithetic and its dip, calculated using the graphs, ranges from around 42º to 60º, so that the higher the amount of extension the higher the shear dip obtained. The estimated shear dips are between 4º and 9º less than those derived from the analysis of the particle trajectories imaged by Edwards (2013). As result, the rollover folds modelled with the calculated parameters are not very different from those of the experiment, overlooking the minor faults the inclined shear model is not able to predict (Figure 16d). The area-based test indicates that the estimated shear dips are less than the correct ones and that the estimated values of extension are slightly larger than the actual ones. But, contrary to the experiments above these differences are slightly smaller for the early stages than for the last stages of the experiment.

The field example analyzed consists of a photograph taken by Maher (2013) of a Triassic normal fault that crops out along a cliff at the Edgeoya island, Svalbard Islands, Norway (Figure 17a). In the slips versus stratigraphic height graph the heave increases stratigraphically downwards, the throw decreases down section and the displacement decreases in the upper stratigraphic horizons and increases in the deepest horizons (Figure 17b). The paths of these functions are similar to those obtained in the theoretical rollovers generated by antithetic shear. The linear best-fit function plotted on the throw versus heave data has a high R-squared parameter value indicating a good fit (Figure 17c), and the differences between the areas of the upper and lower regions according to the method proposed here are not very high. They indicate that the predicted shear dip is slightly less than the correct one and that the estimated extension is a bit greater than the actual one. Therefore, the theoretically predicted horizons do not differ substantially from the actual horizons (Figure 17a). The shear obtained for this particular field example is antithetic and dips around 49º, whereas the estimated extension is around 6100 units.

6.1. Discussion

The analysis of a natural example and different stages of sequential laboratory experiments using the method based on fault slips and the area balancing technique proposed here, points out that: a) the estimated dip of the antithetic shear increases as the amount of extension increases (Figure 18a); b) the calculated shear dip is usually less than that obtained by other methods; c) the shear dips obtained for two experiments (Dula, 1991 and Burger, 2012) are closer to those obtained by other methods as the amount of extension increases, whereas it is the other way round for another experiment (Edwards, 2013); d) the extension value obtained is usually greater than the actual value; e) the extension values obtained for two experiments (Dula, 1991 and Burger, 2012) and the actual ones get closer as the amount of extension augments, whereas it happens on the contrary in the case of another experiment (Edwards, 2013); and f) the results, both for the shear dip and the extension value, are more reliable in stages with greater extension since R-squared for the best-fit functions in the throw versus heave graphs is closer to 1 as the extension value is greater (Figure 18b).

The fact that: a) the shear dip obtained using the method based on fault slips presented in this paper is less than that obtained by other methods that do not employ the slips of horizons, and b) that the estimated extension is greater than the actual values suggests that the best-fit functions obtained in the throw versus heave graphs possess a gentler slope than the one they should supposedly have, and therefore, they intersect with the abscissas axes at higher values. Since we obtained negative slope functions (antithetic shear) for all the analyzed experiments, this could mean that the slips undergone by the higher stratigraphic horizons are, broadly speaking, less than they should be. Alternatively, this could also be explained assuming that the slip values of the stratigraphically deeper horizons are higher than they should be. These observations suggest that additional mechanisms different from vertical/inclined shear may have been active as well.

Whereas rollover folds generated over normal faults linked to detachments are a type of fault-bend folds, the phenomena described above could be interpreted as a result of an initial component of fault-propagation folding in the case of the Dula (1991) experiment; this would cause that slip along the fault would not follow the theoretical pattern expected in a deformation environment dominated by vertical/inclined shear (Figures 4 and 5). Thus, in stages with little extension when the fault is still propagating, upper horizons, whose cut-off points are close to the fault tip, could have suffered a certain slip decrease towards the upper fault termination as a result of the fault-propagation folding component accommodated by both fault propagation and folding. That would explain the low values obtained for the shear dip and its difference from the dip obtained by other methods, the high extension values obtained with respect to the actual extension and the worse results for the initial stages using the slips-based method proposed here. This hypothesis is supported by the fact that in the initial stages of some physical experiments of listric normal faults, such as in the experiment displayed in Cloos (1968), a fault-propagation fold first develops so that the master fault offsets only the lower part of the stratigraphic series and propagates stratigraphically upwards as extension increases (Figures 13 and 14 in Cloos, 1968). The structure ends up becoming a classical rollover fold-type when the master fault is developed all along the stratigraphic sequence (Figures 15 and 16 in Cloos, 1968). Comparable observations have been documented in field examples of listric normal faults. For instance, Uzkeda (2013) shows a 3D model and geological sections across a normal fault in which the hangingwall beds close to the fault dip against it and display a nice rollover geometry in a region where the fault displacement is relatively high (Figure 4.9 B-B' in Uzkeda, 2013). In contrast, in a region where the displacement is less the uppermost beds are almost flat-lying whereas the lower beds dip against the fault (Figures 4.9 A-A' in Uzkeda, 2013). The geometry of the hangingwall beds of this particular fault, very similar to that of the two stages of the Dula (1991) experiment illustrated in figures13a and 13d, could be explained assuming a component of fault-propagation folding during the initial stages of fault development. Drag folding could also be invoked as an additional mechanism to explain the anomalies observed in the fault slips which result in lower shear dips and higher amounts of extension estimations using the slips-based method.

In the case of the Edwards (2013) experiment the low values of shear dip and the high values of extension obtained using the slips-based method, plus the fact that the stages with higher extension supply worse results may be the result of the activity of the crestal collapse graben developed over the rollover anticline. Thus, in the early stages of the experiment, the crestal collapse graben is hardly developed. However, as extension progresses the number of faults that belong to the crestal collapse graben and the displacement along them increases substantially (Figure 16a). The crestal collapse graben faults offset only the upper part of the stratigraphic succession and die out at depth. These faults accommodate part of the extension of the experiment causing a reduction of the displacement suffered by the uppermost stratigraphic horizons along the master fault. This would lead to a gentler slope of the best–fit function that fits the throw versus heave data, and therefore, would result in lower values of shear dip with respect to the dip obtained by other methods and higher values of extension with respect to the actual extension as well as worse results for the last stages of the experiment. Crestal collapse grabens with similar geometrical and kinematical features have been documented in many physical experiments such as those carried out by McClay and coworkers (see references in the introduction section).

Regarding the Burger (2012) experiment, it is unclear whether the low values of shear dip and high values of extension obtained are caused by the occurrence of a fault-propagation folding component as in the Dula (1991) experiment or due to the crestal collapse graben as in the Edwards (2013) experiment. The facts that: a) the crestal collapse graben is developed from the very early stages of the experiment and its degree of development remains approximately constant as extension increases, and b) that the worse results were obtained for the early stages of the experiment suggest that the fault-propagation folding component is a better explanation.

In the sequential physical experiments analyzed, the deduced shear dip seems to increase as extension augments. This suggests that the assumption of one homogeneous vertical/inclined shear direction throughout the deformation process is not valid, at least for these experiments, and that could be one of the reasons why the fit using the proposed method is not as good as it would be desirable. However, the lower reliability of the results obtained in the early stages with respect to the better reliability in the most advanced stages does not allow us to assert this point firmly. Unfortunately, we are unable to check whether this observation is a particular feature of the sequential physical experiments used or it takes place in natural examples as well because different stages of evolution of a structure are unavailable in nature.

If the points exposed above are correct, then we should not expect excellent shear dips and amounts of extension derived from the proposed method because they are averages of deformation fields resulting from various mechanisms, perhaps shear orientations different than vertical/inclined shear, and maybe shear dips that have varied over time. We have to keep in mind that we try to fit functions based on assumptions such as fault-bend folding developed by vertical/inclined, homogeneous shear through time and space to a series of data resulting from more than one process. However, the method can still be used as a guide to decipher how the basic assumptions deviate.

Unfortunately we do not know to what extent these physical experiments emulate correctly natural structures, and therefore, whether the conclusions derived from them can be extrapolated to field and subsurface examples of normal faults that emanate from a detachment. For instance, the physical experiment run by Dula (1991) includes a thin, flexible plastic sheet between the hangingwall and the footwall/basal plate. This film helps with the development of the experiment because it possesses a high slipping coefficient, and therefore, facilitates slip between fault blocks. According to some authors (e.g., Hauge and Gray, 1996), quantitative analysis of physical experiments developed using this particular experimental design, which is an artifact that may not occur in nature, may produce misleading results.

7. Conclusions

In theoretical models of normal faults emanating from a detachment at depth whose hangingwall consists of a rollover fold deformed by vertical or inclined shear, a pattern for the variation of the displacement along the fault, heave and throw has been recognized. For the horizon located on the detachment the throw is zero, and the heave and the fault displacement are equal, and equal to the horizontal extension. The linear best-fit of the data for several horizons plotted on a throw versus heave graph supplies quantitative information about the shear (character and dip) and the amount of extension responsible for the rollover formation. The slope of such function is the tangent of the shear dip (positive slope for synthetic, negative for antithetic and infinite for vertical shear) and its intersection with the x-axis is the amount of extension.

By using data from the upper part of a stratigraphic sequence offset by a normal fault, the proposed method would allow to estimate the character and dip of the shear, as well as the amount of extension to produce the analyzed rollover. In addition, for those cases in which the complete geometry of the fault is known, an area-based method has been presented that allows us to estimate whether the shear dip and amount of extension calculated are higher or lower than the correct values. Both the throw versus heave and slips versus stratigraphic height graphs would enable recognizing mechanisms additional to vertical or inclined shear. If that is the case, the graphs would not follow the patterns deduced from the theoretical models. This observation is of major importance when attempting to reconstruct, restore and/or forward model structures since the proposed tool supplies valuable information regarding the selection of the most appropriate algorithms.

The proposed method is still valid when reverse reactivation of a normal fault with the same shear dip takes place. If the inversion is partial the graphs permit to obtain both the shear dip and the remnant extension at present-day. In the case of total inversion, a certain amount of reverse slip would appear and the graphs would allow to calculate the shear dip and the net contraction. If sediments pre-extension and post-extension pre-inversion are preserved, it is possible to calculate the shear dip, the remnant extension, the contraction and, by adding both, the total extension.

The application of the proposed method to a natural example and different stages of sequential physical experiments of rollovers related to normal listric faults, and verification of the results using a method based on comparing areas, permits to extract the following conclusions: a) the shear dip obtained using the slips-based method are minimum estimates, and b) the extension values calculated are maximum estimates. In those cases where the greater the amount of extension undergone by the structures the more accurate both the shear dip and amount of extension estimates, these points have been explained assuming that the generation of rollovers include a certain component of fault-propagation folding (and/or drag folding) in the early stages of the experiments whose effects ameliorate as cut-off points of horizons in the hangingwall approach the detachment. In those cases in which the better results are obtained for the early stages of the experiment, these points have been related to the development of a crestal collapse graben that becomes more active as extension progresses. In addition, the analysis of the experiments shows that the shear dip is not uniform during the extensional process but seems to increase as the extension progresses. All these observations led us to state that we should not expect obtaining excellent shear dips and amounts of extension using the slips-based method proposed because these results are averages of deformation fields resulting from various processes, but the method is still useful as a guide on checking how the basic assumptions of rollover folds formed by vertical/inclined shear deviate in each particular example analyzed.

8. Acknowledgements

The authors would like to acknowledge financial support by research projects CGL 2011-23628 (Desarrollo de fracturas and venas asociadas al plegamiento -FRAVEPLE-) and CSD 2006-0041 (Geociencias en Iberia: estudios integrados de topografía y evolución 4D -TOPO-IBERIA-) funded by diverse Spanish Ministries. H. Uzkeda thanks the support by the Spanish Ministry of Education via an FPU grant partially funded by the European Social Fund. We would like to thank the editor Thomas Blenkinsop as well as the reviewers (Chris Connors and an anonymous one) for constructive comments which substantially improved the manuscript.

REFERENCES

Barr, D., 1985. 3-D palinspastic restoration of normal faults in the inner Moray Firth: implication for extensional basin development. Earth and Planetary Science Letters 75, 191-203.

Bulnes, M., Poblet, J., 1999. Estimating the detachment depth in cross sections involving detachment folds. Geological Magazine 136, 395-412.

Burger, R., 2012. Evolution of normal fault systems during progressive deformation. Teaching Structural Geology in the 21st Century [Online]. Science Education Resource Center at Carleton College. Available: http://serc.carleton.edu/NAGTWorkshops/structure04/activities/3861.html [Accessed 4 April 2014]

Chamberlin, R.T., 1910. The Appalachian folds of Central Pennsylvania. Journal of Geology 18, 228-251.

Chapman, T.J., Williams, G.D., 1984. Displacement-distance methods in the analysis of fold-thrust structures and linked-fault systems. Journal of the Geological Society 141, 121-128.

Cloos, E., 1968. Experimental analysis of Gulf Coast fracture patterns. American Association of Petroleum Geologists Bulletin 52, 420-444.

Davison, I., 1986. Listric normal fault profiles: calculation using bed-length balance and fault displacement. Journal of Structural Geology 8, 209-210.

Dula, W.F., 1991. Geometric models of listric normal faults and rollover folds. American Association of Petroleum Geologists Bulletin 75, 1609-1625.

Edwards, R., 2013. Scaled analogue modelling of rift systems. MSc Dissertation. Royal Holloway, University of London. 113 p.

Ellis, P.G., McClay, K.R., 1988. Listric extensional fault systems; results of analogue model experiments. Basin Research 1, 55-70.

Groshong, R.H., 1989. Half-graben structures; balanced models of extensional fault-bend folds. Geological Society of America Bulletin 101, 96-105.

Groshong, R.H., 1990. Unique determination of normal fault shape from hanging-wall bed geometry in detached half grabens. Eclogae Geologicae Helvetiae 83, 455-471.

Groshong, R.H., 1994. Area balance, depth to detachment, and strain in extension. Tectonics 13, 1488-1497.

Groshong, R.H., 1996. Construction and validation of extensional cross-sections using lost area and strain, with application to the Rhine Graben. In: Buchanan, P.G., Nieuwland, D.A. (Eds.), Modern developments in structural interpretation, validation and modeling. Geological Society Special Publications 99, 79-87.

Gwinn, V.E., 1970. Kinematic patterns and estimates of lateral shortening. Valley and Ridge and Great Valley Provinces, Central Appalachians, South-Central Pennsylvania. In: Fisher, G.W.; Pettijohn, F.J.; Reed, J.C., Weaver, K.N. (Eds.), Studies of Appalachian Geology: central and southern. Wiley, New York, 127-146.

Hauge, T.A., Gray, G.G. 1996. A critique of techniques for modelling normal-fault and rollover geometries. In: Buchanan, P.G., Nieuwland, D.A. (Eds.): Modern developments in structural interpretation, validation and modelling. Geological

Society Special Publication, 99, 89-97.

Henza, A.A., Withjack, M.O., Schlische, R.W., 2010. Normal-fault development during two phases of non-coaxial extension: An experimental study. Journal of Structural Geology 32, 1656-1667.

Jackson, M., Galloway, W., 1984. Structural and depositional styles of Gulf Coast Tertiary continental margins: application to hydrocarbon exploration. American Association of Petroleum Geologists Educational Course Notes 25: 1-150.

Maher, H.D.Jr., 2013. Structures in extensional terranes. Structural Geology Course (GEOL 3300). [Online]. Available: http://maps.unomaha.edu/maher/GEOL3300/week14/rift.html#anchor343867 [Accessed 3 April 2014]

Matos, R.M.D. de, 1993. Geometry of the hanging wall above a system of listric normal faults – A numerical solution. American Association of Petroleum Geologists Bulletin 77, 1839-1859.

McClay, K.R., 1989. Physical models of structural styles during extension. In: Tankard, A.J., Balkwill, H.R. (Eds.): Extensional Tectonics and Stratigraphy of the North Atlantic Margins. American Association of Petroleum Geologists Memoir 46, 95-110.

McClay, K.R., 1990a. Deformation mechanics in analogue models of extensional fault systems. In: Knipe, R.J., Rutter, E.H. (Eds.): Deformation mechanisms, rheology and tectonics. Geological Society Special Publications 54, 445-453.

McClay, K.R., 1990b. Extensional fault systems in sedimentary basins; a review of analogue model studies. Marine and Petroleum Geology 7, 206-233.

McClay, K.R., 1995. 2D and 3D analogue modeling of extensional fault structures; templates for seismic interpretation. Petroleum Geoscience 1, 163-178.

McClay, K.R., 1996. Recent advances in analogue modeling; uses in section interpretation and validation. In: Buchanan, P.G., Nieuwland, D.A. (Eds.): Modern developments in structural interpretation, validation and modeling. Geological Society Special Publications 99, 201-225.

McClay, K.R., Ellis, P.G., 1987a. Analogue models of extensional fault geometries. In: Coward, M.P.; Dewey, J.F., Hancock, P.L. (Eds.), Continental extensional tectonics. Geological Society Special Publications 28, 109-125.

McClay, K.R., Ellis, P.G., 1987b. Geometries of extension fault systems developed in model experiments. Geology 15, 341-344.

McClay, K.R., Waltham, D.A., Dooley, T., Deeks, N., Willacy, C., 1995. Fault reconstruction techniques. Fault Dynamics Project Short Course, 183-192.

Moretti, I., Colletta, B., Vially, R., 1988. Theoretical model of block rotation along circular faults. Tectonophysics 153, 313-320.

Morris, A.P., Ferrill, D.A., 1999. Constant-thickness deformation above curved normal faults. Journal of Structural Geology 21, 67-83.

Poblet, J., Bulnes, M., 2005ba Estimating extension and depth to detachment in simple rollover anticlines over listric normal faults. Trabajos de Geología 25, 85-100.

Poblet, J., Bulnes, M., 2005b. Fault-slip, bed-length and area variations in experimental rollover anticlines over listric normal faults: influence in extension and depth to detachment estimations. Tectonophysics 396, 97-117.

Poblet, J., Bulnes, M., 2007. Predicting strain using forward modelling of restored cross-sections; application to rollover anticlines over listric normal faults. Journal of Structural Geology 29, 1960-1970.

Schlische, R.W., Withjack, M.O., Eisenstadt, G., 2002. An experimental study of the secondary deformation produced by oblique-slip normal faulting. American Association of Petroleum Geologists Bulletin 86, 885-906.

Song, T., Cawood, P.A., 2001. Effects of subsidiary faults on the geometric construction of listric normal fault systems. American Association of Petroleum Geologists Bulletin 85, 221-232.

Tearpock, D.J., Bischke, R.E., 1991. Applied subsurface geological mapping. Prentice Hall, New Jersey.

Uzkeda, H., 2013. Reconstrucción 3D y análisis estructural de las rocas jurásicas de Colunga-Tazones (Cuenca Asturiana, NO de la Península Ibérica). PhD thesis, Universidad de Oviedo, 244 p.

Verrall, P., 1981. Structural interpretation with application to North Sea problems. Joint Association of Petroleum Exploration Courses (JAPEC). Course Notes 3.

Waltham, D., 1989. Finite difference modeling of hangingwall deformation. Journal of Structural Geology 11, 433-437.

White, N.J., Jackson, J.A., McKenzie, D.P., 1986. The relationship between the geometry of normal faults and that of the sedimentary layers in their hanging walls. Journal of Structural Geology 8, 897-909.

White, N.J., Yielding, G., 1991. Calculating normal fault geometries at depth: theory and examples. In: Roberts, A.M., Yielding, G., Freeman, B. (Eds.), The geometry of normal faults. Geological Society Special Publications 56, 251-260.

Williams, G., Vann, I., 1987. The geometry of listric normal faults and deformation in their hangingwalls. Journal of Structural Geology 9, 789-795.

Xiao, H., Suppe, J., 1992. Origin of rollover. American Association of Petroleum Geologists Bulletin 76, 509-529.

Ziegler, P.A., 1982. Faulting and graben formation in western and central Europe. In: Kent, P., Botts, M.H.P., McKenzie, D.P., Williams, C.A. (Eds.), Evolution of sedimentary basins. Philosophical Transactions of the Royal Society of London Series A Mathematical and Physical Sciences 305, 113-143.

FIGURE CAPTIONS

Figure 1. Examples of listric normal faults reconstructed at depth through different methods using the same rollover geometry as input data: a) flexural slip; b) constant displacement; c) antithetic shear of 80º dip; d) vertical shear and e) synthetic shear of 80º dip.

Figure 2. Examples of rollover folds generated with antithetic shear of 80º dip in the hangingwall of different shape faults: a) ramp-flat, b) segments of constant dip, c) arctangent function, d) spline, and e) cubic function.

Figure 3. a) Example of a rollover fold constructed with antithetic shear of 80º dip illustrating the measurements (stratigraphic height, heave, throw and displacement) that must be taken for each horizon offset by the fault. These values are plotted on two graphs: b) fault slip (heave, throw and displacement) versus stratigraphic height and c) throw versus heave. The position of the reference level is arbitrary and it is used to measure the stratigraphic height of each horizon. The different stratigraphic horizons are labelled as a, b, c, d, e, f, g and h in a), b) and c).

Figure 4. Graphs for rollover folds formed above planar ramp-flat normal faults created with: a) vertical shear, b) antithetic shear of 80º dip and c) synthetic shear of 80º dip. The fault and rollover fold shape are shown inside the grey rectangle. The arbitrary reference level chosen is the highest stratigraphic horizon. The measurements have been taken according to the procedure illustrated in figure 3.

Figure 5. Graphs for rollover folds related to listric normal faults created using the arctangent function constructed with: a) vertical shear, b) antithetic shear of 80º dip and c) synthetic shear of 80º dip. The fault and rollover fold shapes are

shown inside the grey rectangle. The arbitrary reference level chosen is the highest stratigraphic horizon. The measurements have been taken according to the procedure illustrated in figure 3.

Figure 6. Relation between the throw, heave and extension in rollovers related to listric normal faults generated by: a) antithetic shear and b) synthetic shear. e: amount of extension, h: heave, t: throw, and α: shear dip.

Figure 7. Graphs for rollover folds developed above listric normal faults constituted by segments of constant dip constructed maintaining constant both bed lengths and thicknesses, following the methods of: a) Morris and Ferrill (1999) and b) Davison (1986). The fault and rollover fold shape are shown inside the grey rectangle. The arbitrary reference level chosen is the highest stratigraphic horizon. The measurements have been taken according to the procedure illustrated in figure 3.

Figure 8. Calculation of the amount of extension and the shear angle using the throw versus heave graphs. The fault and rollover fold shape used are shown inside the grey rectangle. The measurements have been taken according to the procedure illustrated in figure 3.

Figure 9. Area-based procedure to check whether the values of shear dip and extension estimated using the slips-based method proposed in this paper are correct for those cases in which the full geometry of the fault is known. a) Present-day, deformed section and b) undeformed section. Present-day, deformed section overlapped onto the undeformed section constructed with synthetic shear of 80º dip (c), vertical shear (d), and antithetic shear of 80º dip (e) and 45º dip (f), and comparison of the areas of the upper, triangular zone and lower zone.

Figure 10. Graphs for folds developed over listric normal faults that underwent reverse reactivation greater than the initial extensional motion: a) inversion by shear with equal dip to that of extension (antithetic shear of 80º dip); b) inversion by shear with a dip different to that of extension (extension with antithetic shear of 80º dip and contraction with antithetic shear of 60º dip); c) extension following the flexural slip method of Davison (1986) and inversion with inclined shear (antithetic shear of 80º dip). The fault and rollover fold shape are shown inside the grey rectangle. The arbitrary reference level chosen is the highest stratigraphic horizon. The measurements have been taken according to the procedure illustrated in figure 3.

Figure 11. Graphs for a fold developed over a listric normal fault including pre-extension and syn-extension beds: a) slips versus stratigraphic height graph and b) throw versus heave graph. The fault and rollover fold shape are shown in the inside figure below the slips versus stratigraphic height graph. The arbitrary reference level chosen is the highest stratigraphic horizon. The measurements have been taken according to the procedure illustrated in figure 3.

Figure 12. Graphs for a fold developed over a listric normal fault that underwent a positive tectonic inversion including pre-extension, syn-extension, post-extension pre-inversion, and syn-inversion beds: a) slips versus stratigraphic height graph, b) throw versus heave graph, c) throw versus heave graph for the pre-extension horizons and d) throw versus heave graph for the post-extension pre-inversion horizons. The fault and rollover fold shape are shown in the inset figure below the slip versus stratigraphic height graph. The arbitrary reference level chosen is the highest stratigraphic horizon. The measurements have been taken according to the procedure illustrated in figure 3.

Figure 13. Results obtained for photographs of the clay experiment of figures 5d and 7a in Dula (1991) consisting of a rollover developed above a listric normal fault. a) and d) Line drawings of two different stages of the experiment derived from photographs, including the beds employed to construct the graphs and the modelled upper horizon; b) and e) slip versus stratigraphic height graphs for the experiment depicted in a) and d) respectively; and c) and f) throw versus heave graphs for the experiment depicted in a) and d) respectively. The arbitrary reference level chosen is the highest stratigraphic horizon. The measurements have been taken according to the procedure illustrated in figure 3.

Figure 14. Application of the area-based procedure to the a) less evolved and to the b) more evolved stages of the Dula (1991) experiment. The areas of the lower regions are greater than those of the upper regions, specially for the less evolved stage of the experiment, suggesting that the estimated shear dip is gentler than the correct value and that the estimated extension is larger than the actual one. The measurements have been taken according to the procedure illustrated in figure 3.

Figure 15. Results obtained for a series of photographs from a sand experiment by Burger (2012) consisting of a rollover developed above a listric normal fault. a) Line drawing of the experiment derived from the photographs, b) slip versus stratigraphic height graphs, c) throw versus heave graphs, d) comparison between the experimental upper horizons and the modelled ones, and e) comparison between the extension increments of the experiment and the modelled ones for the last five stages (taking the third stage as reference). The arbitrary reference level chosen is the highest stratigraphic horizon. The measurements have been taken according to the procedure illustrated in figure 3.

Figure 16. Results obtained for a series of photographs from a sand experiment by Edwards (2013) consisting of a rollover developed above a listric normal fault. a) Line drawings of the experiment derived from photographs, b) slip versus stratigraphic height graphs, c) throw versus heave graphs, and d) comparison between the experimental upper horizons and the modelled ones. The arbitrary reference level chosen is the highest stratigraphic horizon. The measurements have been taken according to the procedure illustrated in figure 3.

Figure 17. Results obtained for a photograph taken by Maher (2013) of a field example of a rollover developed above a listric normal fault. a) Geological interpretation of the photograph, including the beds employed to construct the graphs and the modelled horizons; b) slip versus stratigraphic height graph, and c) throw versus heave graph. The arbitrary reference level chosen is the highest stratigraphic horizon. Since no scale is available in the photograph we assigned arbitrary units. The measurements have been taken according to the procedure illustrated in figure 3.

Figure 18. Plots of a) the shear dip and b) the R-squared parameter obtained for the different stages of the physical experiments analyzed in this study versus extension.

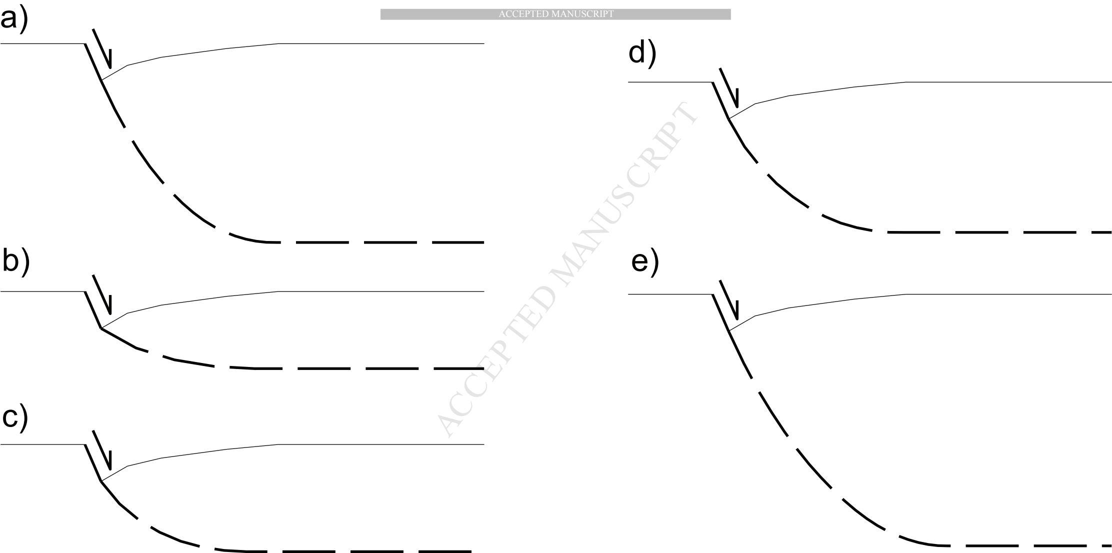
a)
b)
c)
d)
e)

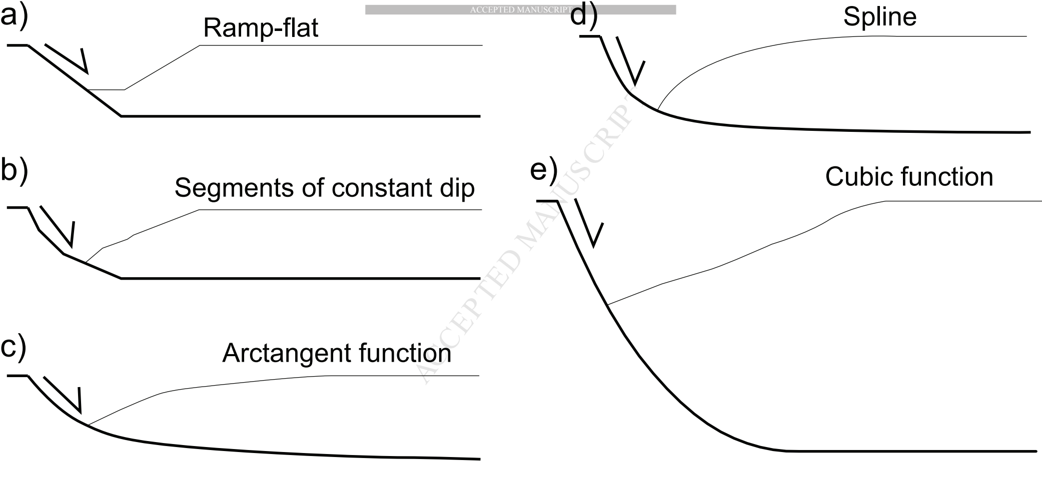
a)
Ramp-flat
b)
Segments of constant dip
c)
Arctangent function
d)
Spline
e)
Cubic function

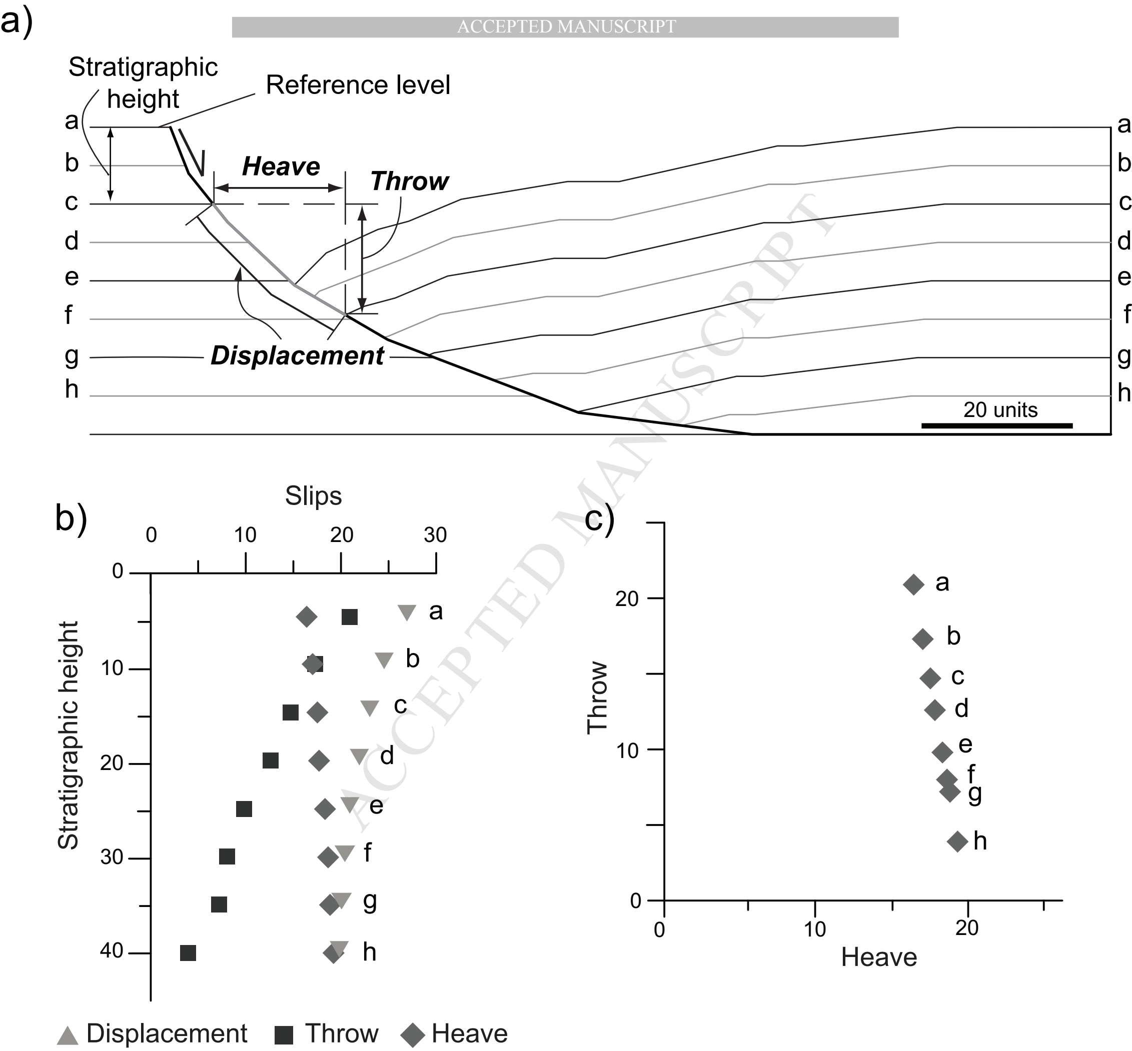
a)
Stratigraphic height
Reference level
Heave
Throw
Displacement
a
b
c
d
e
f
g
h
20 units
b)
Slips
0
10
20
30
Stratigraphic height
0
10
20
30
40
c)
Throw
Heave
Displacement
Throw
Heave

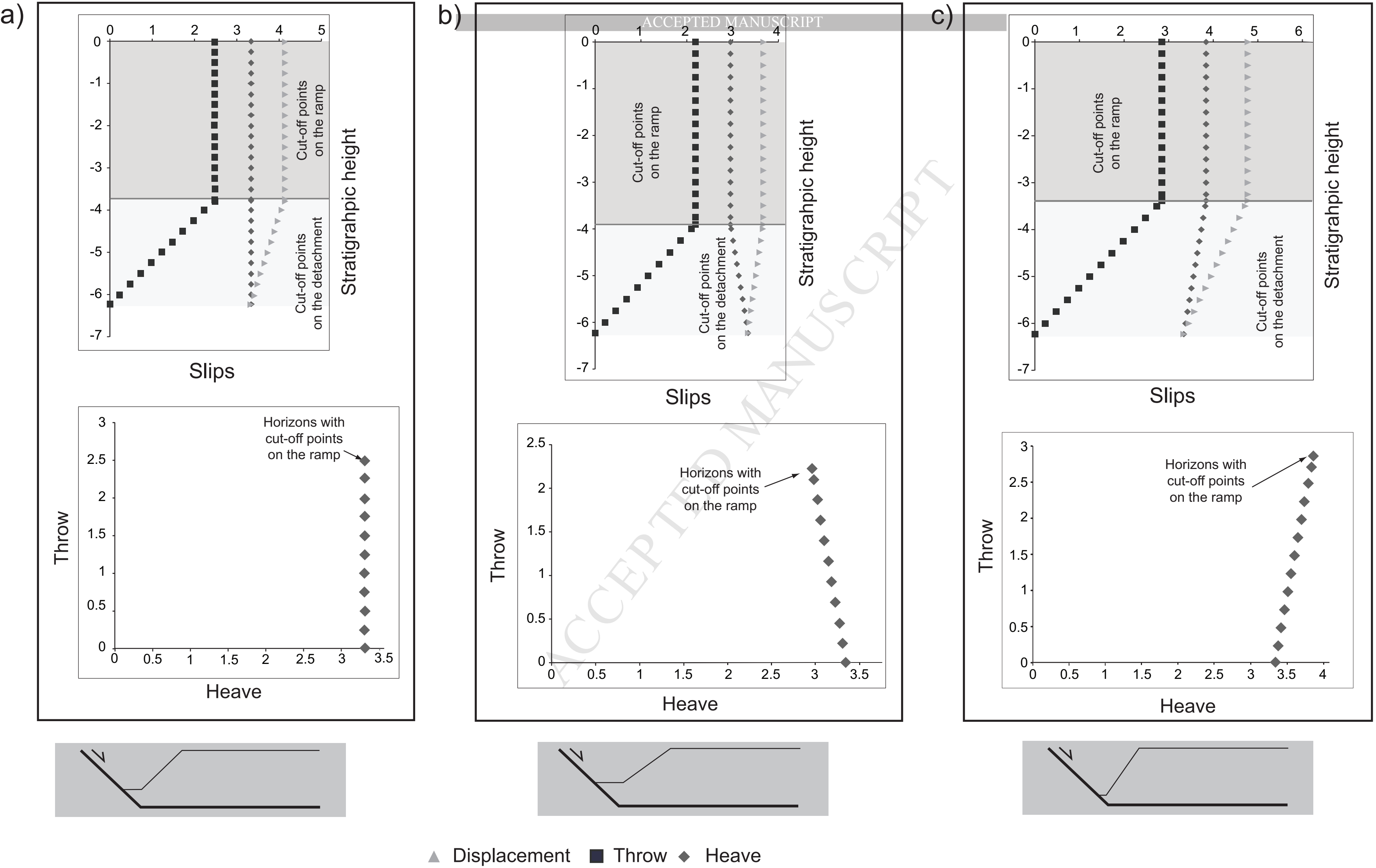

a)
b)
c)
Cut-off points on the ramp
Cut-off points on the detachment
Stratigrahpic height
Slips
Horizons with cut-off points on the ramp
Throw
Heave
Displacement
Throw
Heave

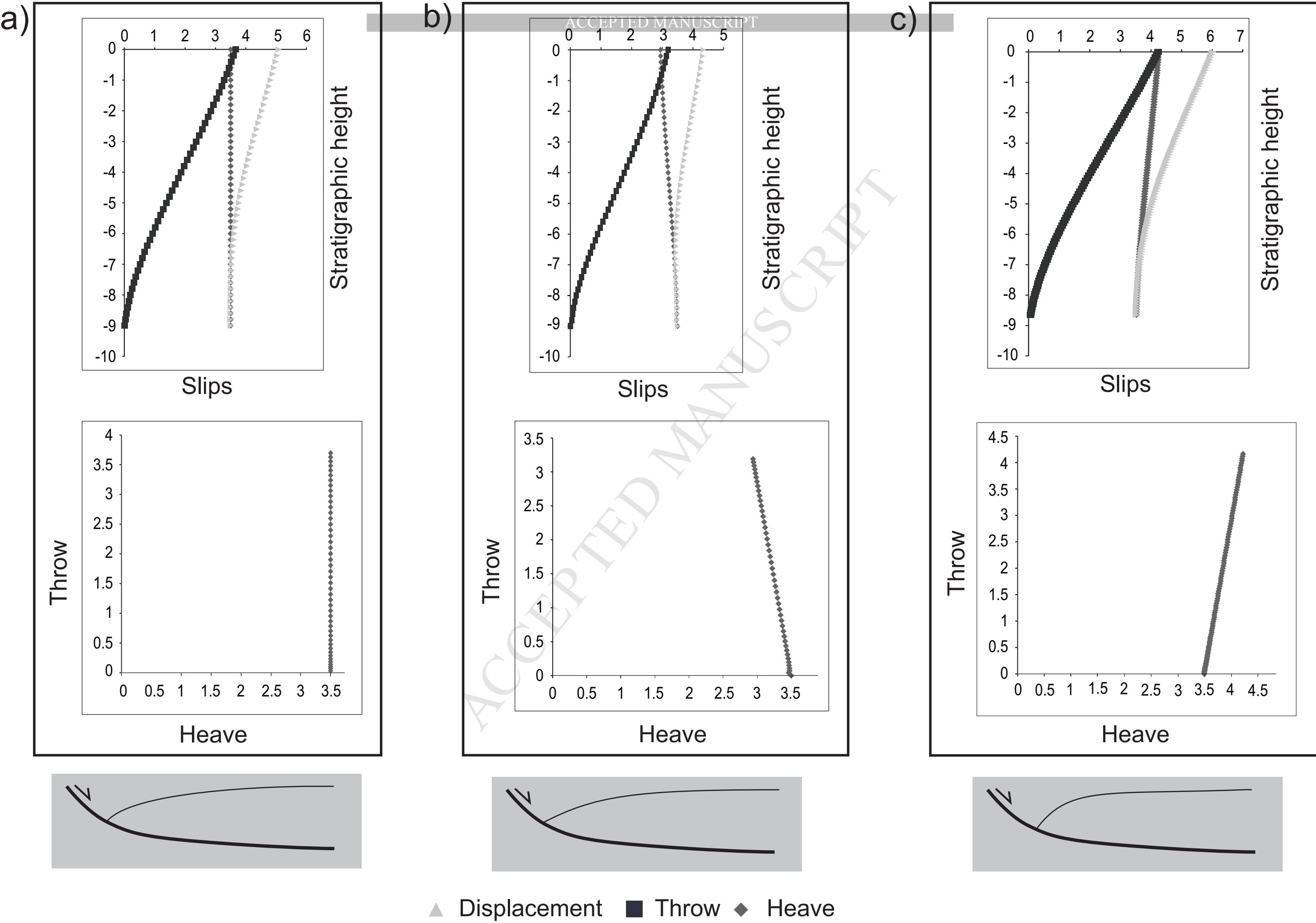
a)
b)
c)
Stratigraphic height
Slips
Throw
Heave
Displacement
Throw
Heave

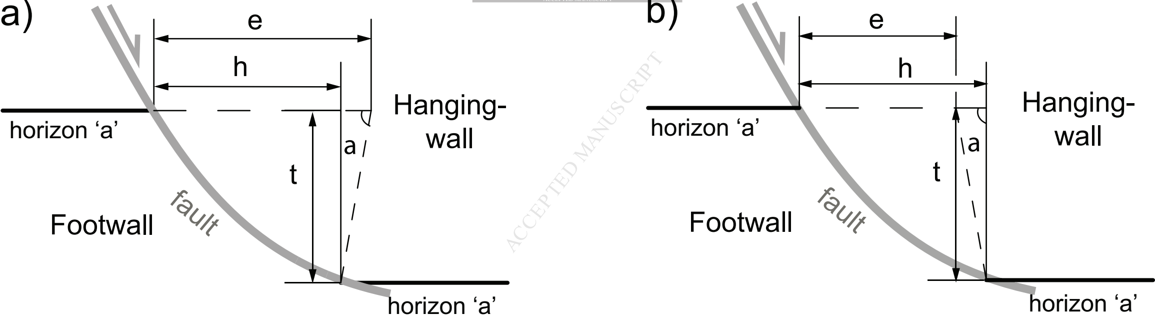
a)
e
h
Hanging-
wall
horizon 'a'
a
t
Footwall
fault
horizon 'a'
b)
e
h
Hanging-
wall
horizon 'a'
a
t
Footwall
fault
horizon 'a'

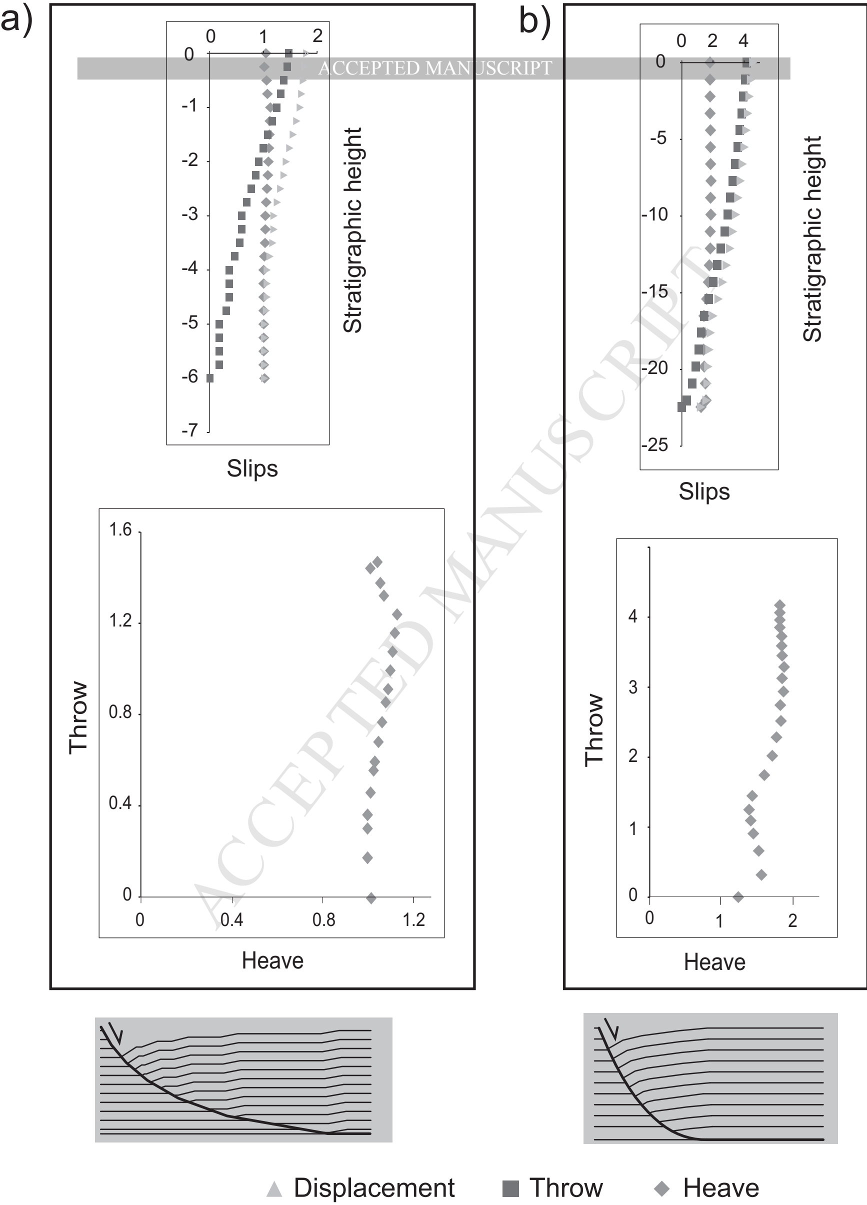
a)
b)
Stratigraphic height
Slips
Throw
Heave
Displacement
Throw
Heave

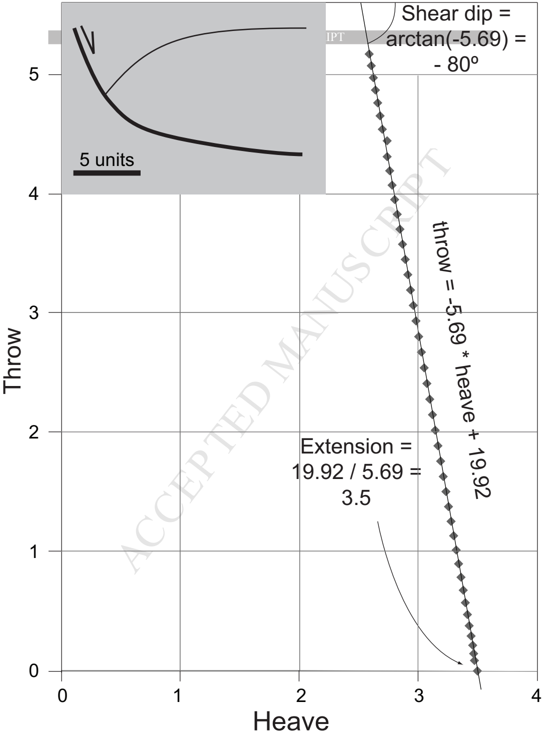

Shear dip =
arctan(-5.69) =
- 80º
5 units
throw = -5.69 * heave + 19.92
Extension =
19.92 / 5.69 =
3.5
Throw
Heave
0
1
2
3
4
5
0
1
2
3
4

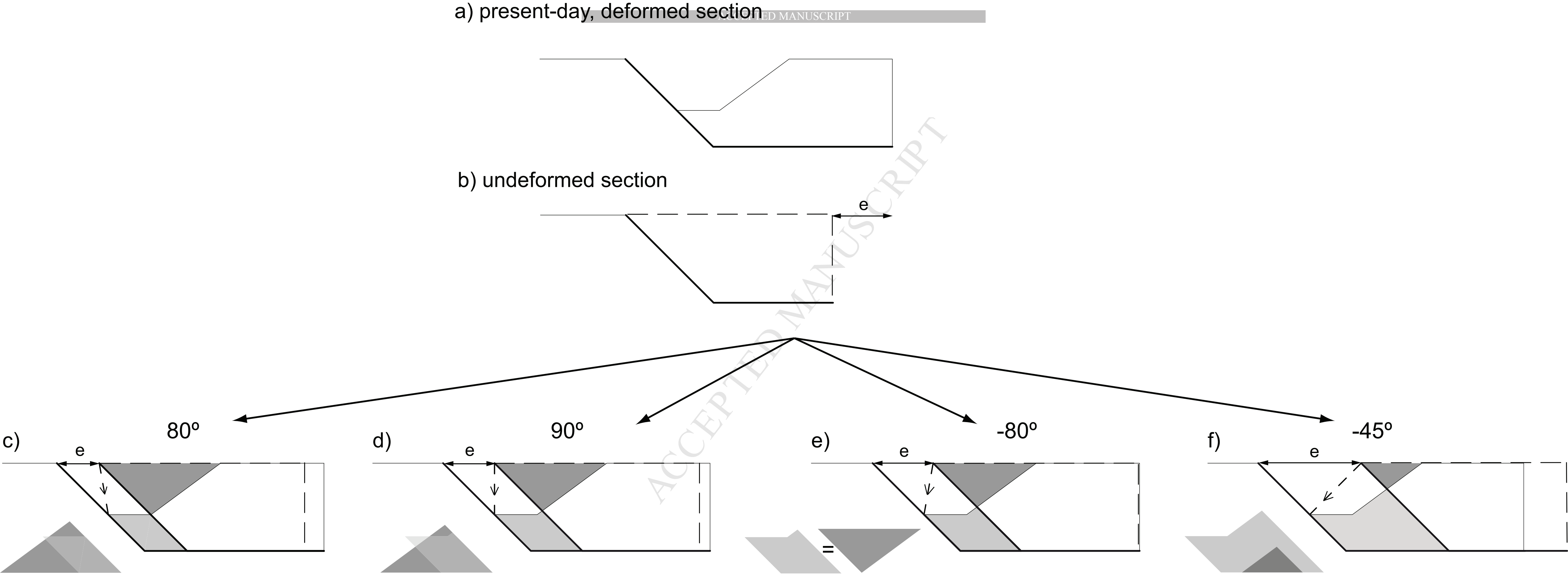

a) present-day, deformed section
b) undeformed section
e
c)
80º
e
d)
90º
e
e)
-80º
e
=
f)
-45º
e

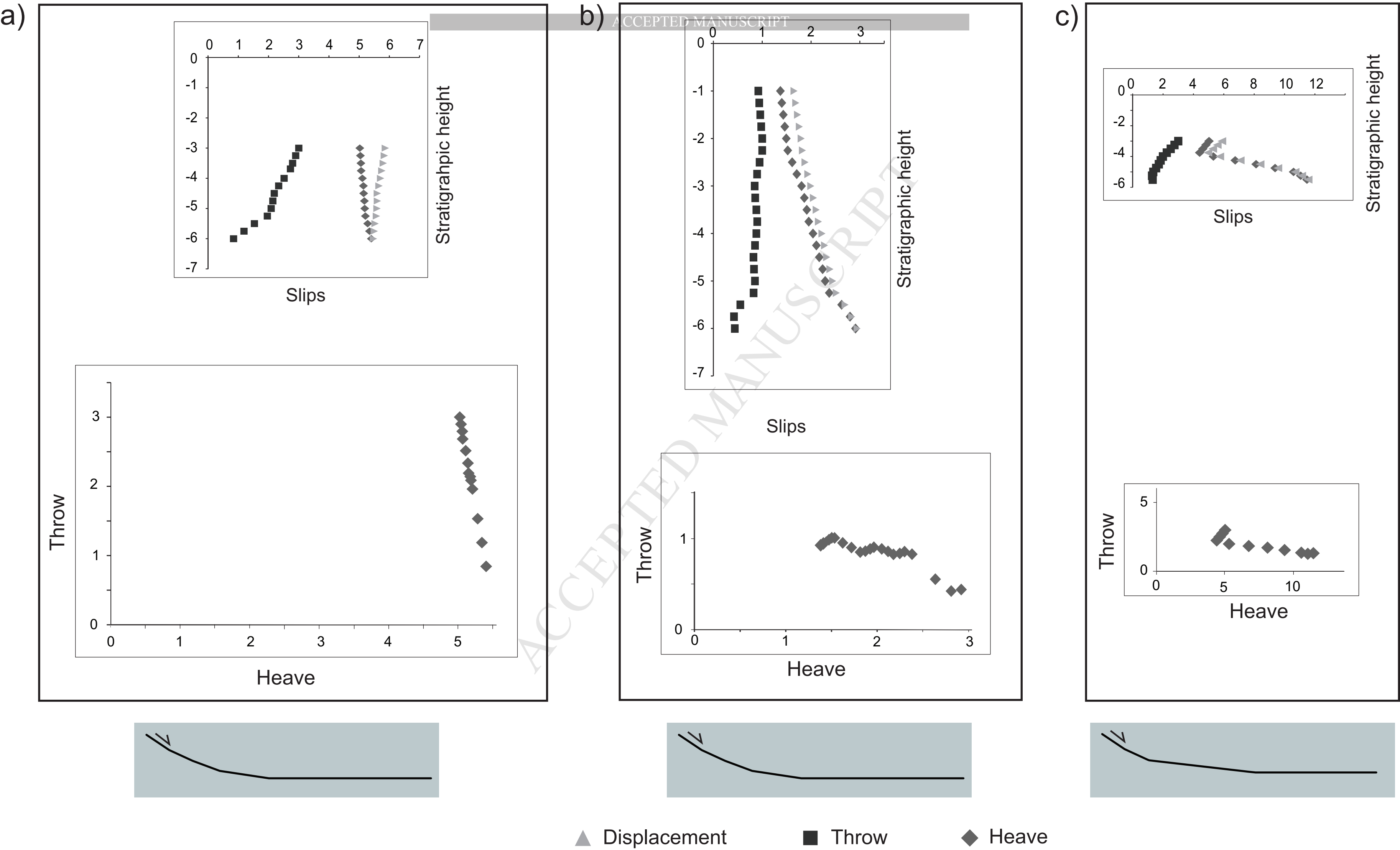
a)
Slips
Stratigrahpic height
Throw
Heave
b)
Slips
Stratigraphic height
Throw
Heave
c)
Slips
Stratigraphic height
Throw
Heave
Displacement
Throw
Heave

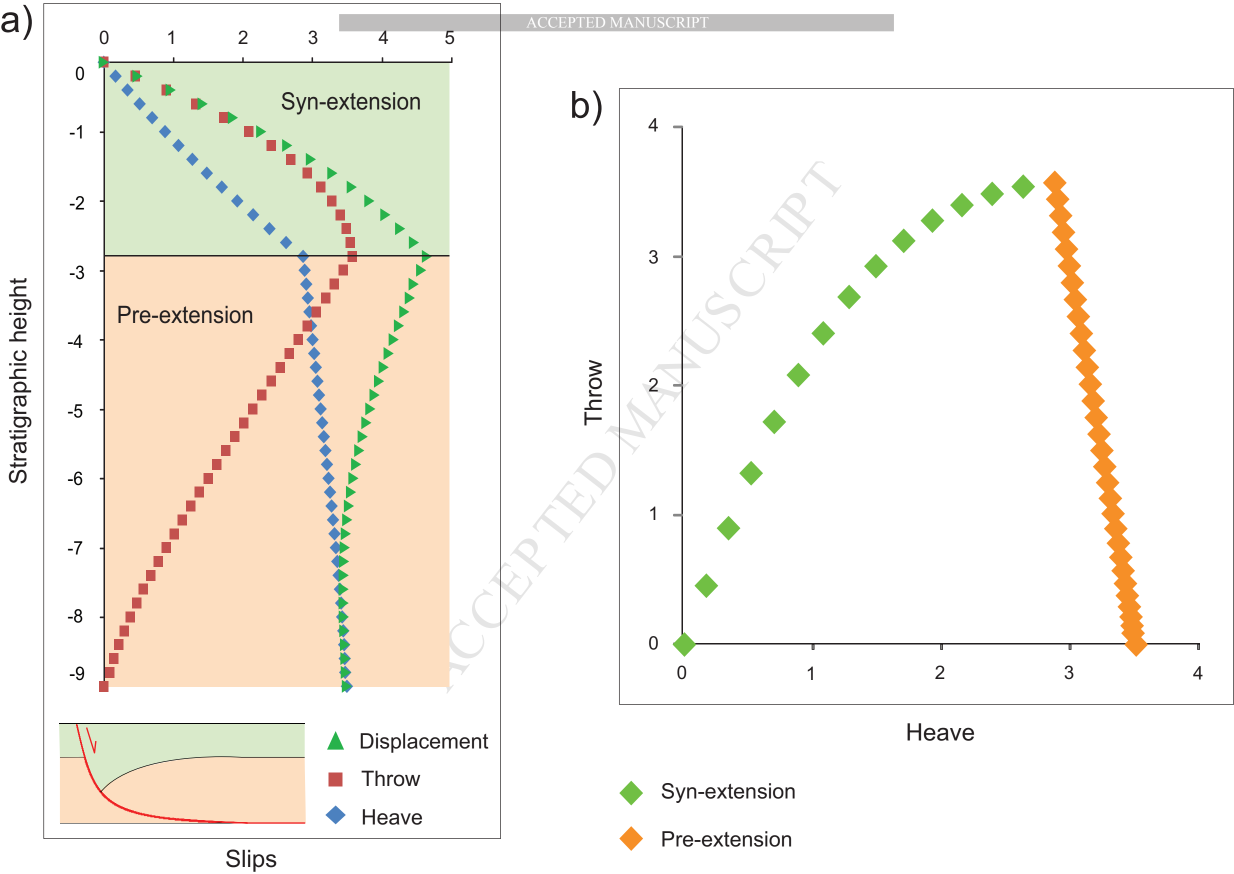

a)
0
1
2
3
4
5
0
-1
-2
-3
-4
-5
-6
-7
-8
-9
Syn-extension
Pre-extension
Stratigraphic height
Displacement
Throw
Heave
Slips
b)
4
3
2
1
0
0
1
2
3
4
Throw
Heave
Syn-extension
Pre-extension

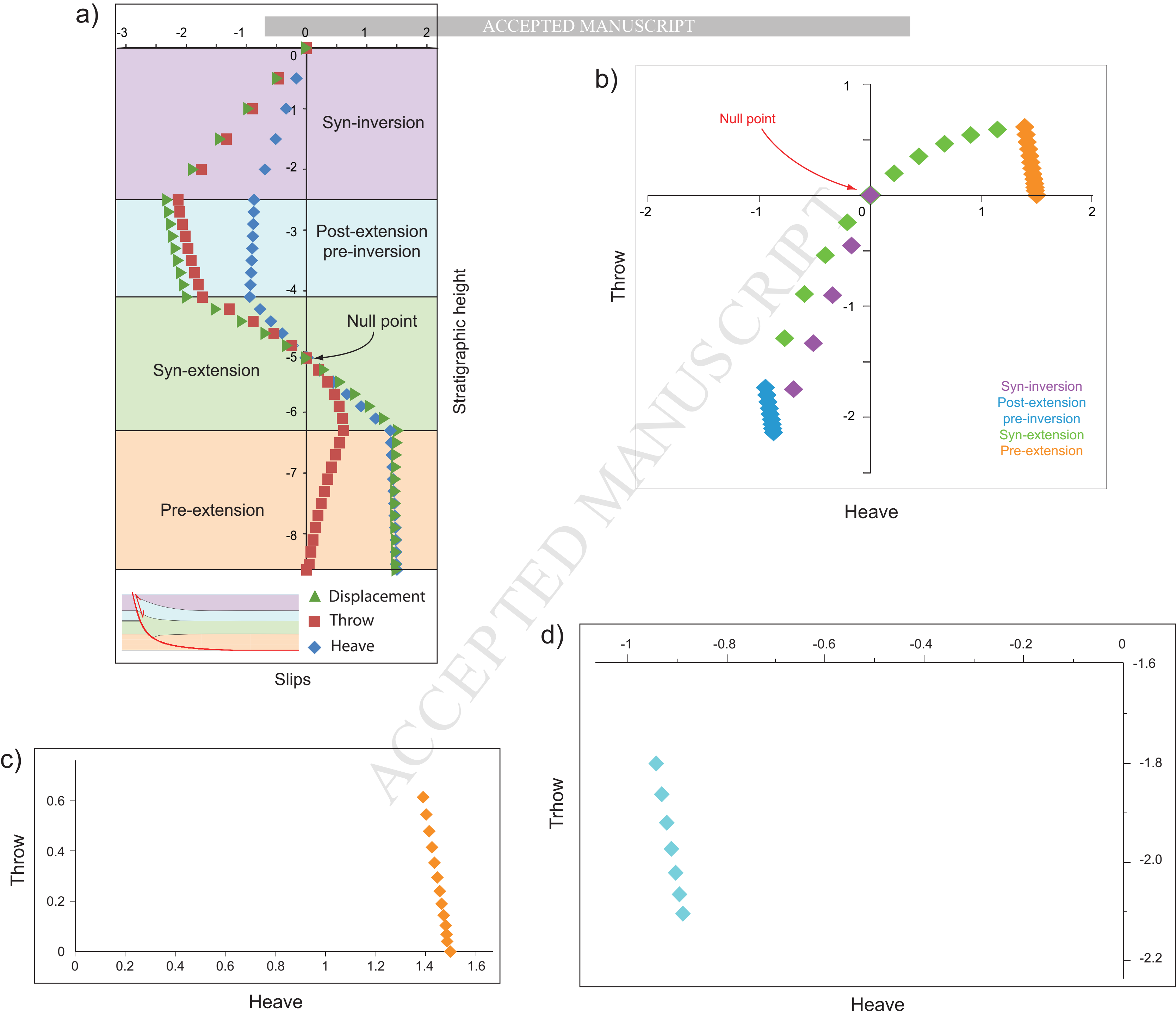

a)
Syn-inversion
Post-extension
pre-inversion
Syn-extension
Null point
Pre-extension
Stratigraphic height
Displacement
Throw
Heave
Slips
b)
Null point
Throw
Heave
Syn-inversion
Post-extension
pre-inversion
Syn-extension
Pre-extension
c)
Throw
Heave
d)
Trhow
Heave

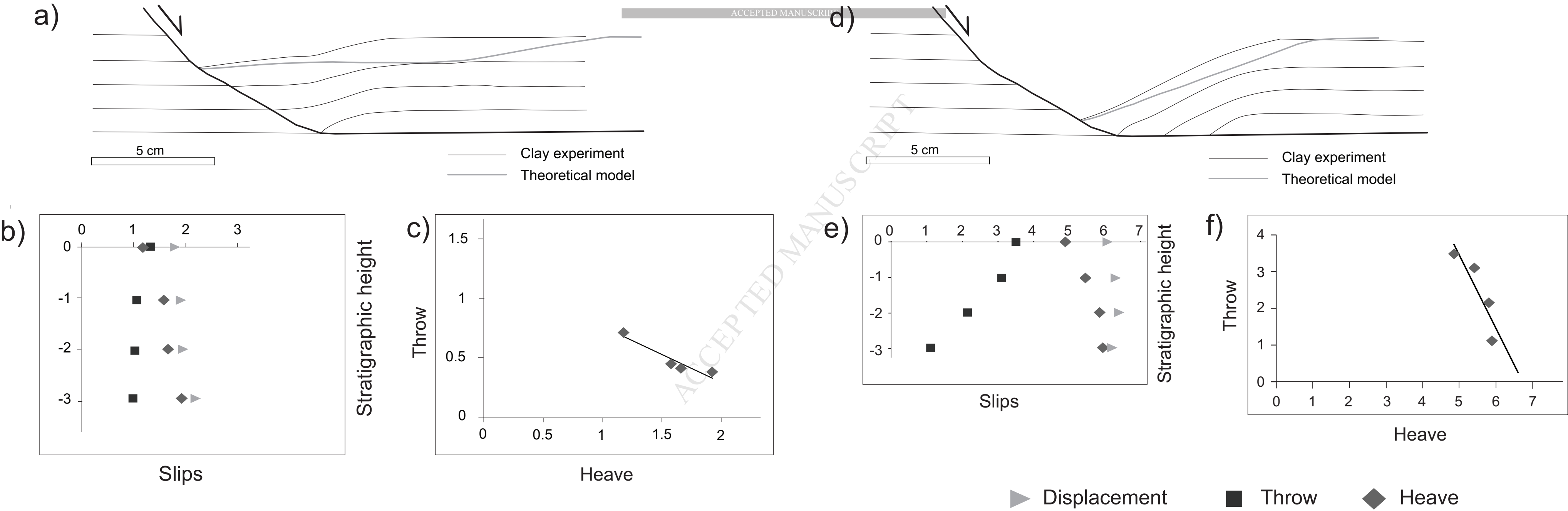

a)
5 cm
Clay experiment
Theoretical model
d)
5 cm
Clay experiment
Theoretical model
b)
0
1
2
3
0
-1
-2
-3
Slips
Stratigraphic height
c)
1.5
1
0.5
0
Throw
0
0.5
1
1.5
2
Heave
e)
0
1
2
3
4
5
6
7
0
-1
-2
-3
Slips
Stratigraphic height
f)
4
3
2
1
0
Throw
0
1
2
3
4
5
6
7
Heave
Displacement
Throw
Heave

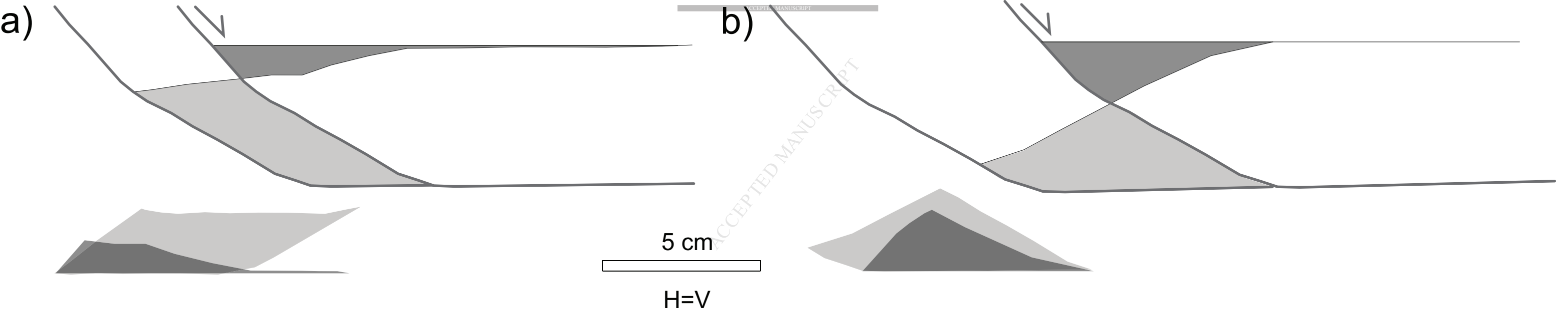
a)
b)
5 cm
H=V

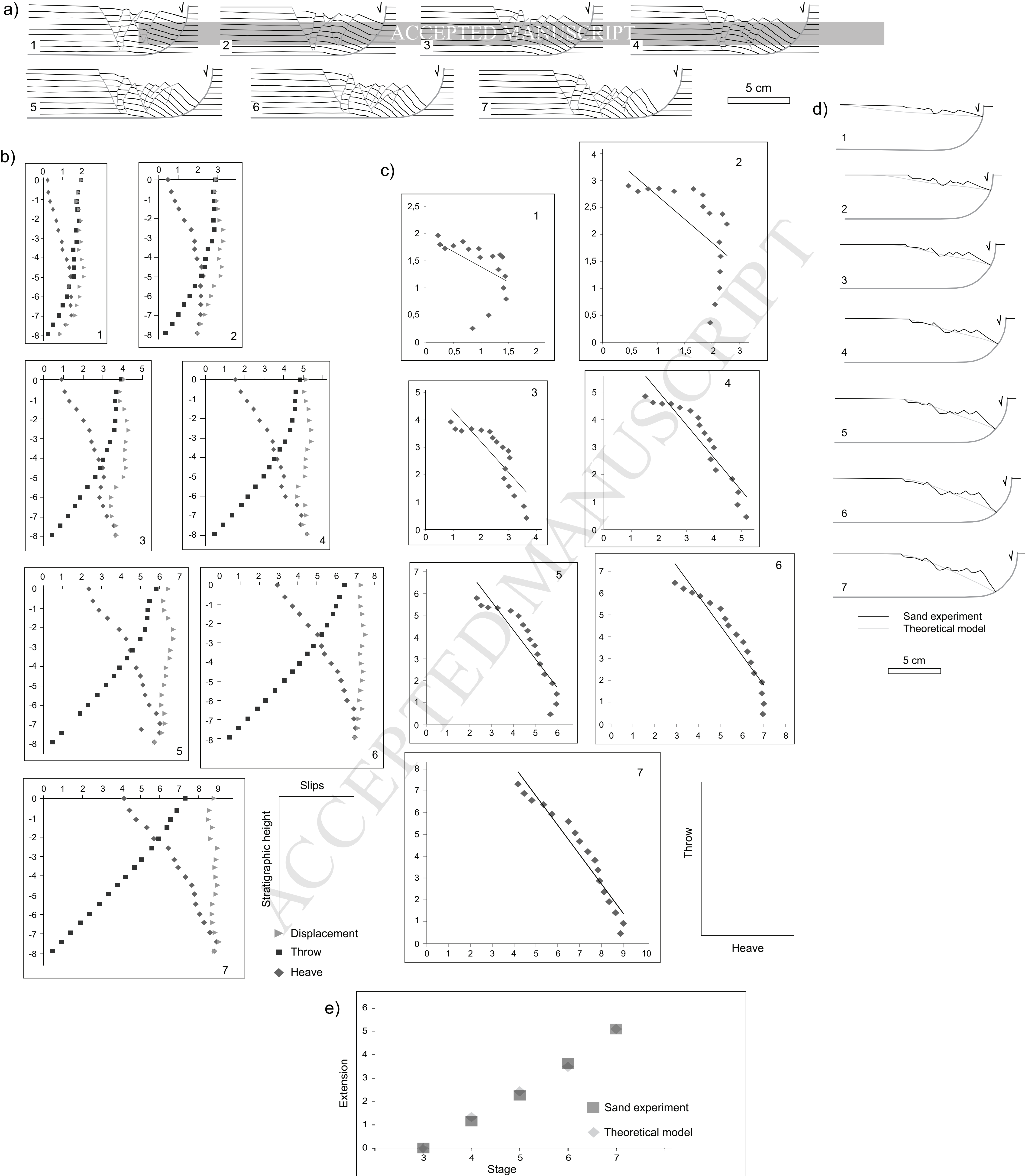

a)
5 cm
b)
c)
d)
Sand experiment
Theoretical model
5 cm
Slips
Stratigraphic height
Displacement
Throw
Heave
Throw
Heave
e)
Extension
Stage
Sand experiment
Theoretical model

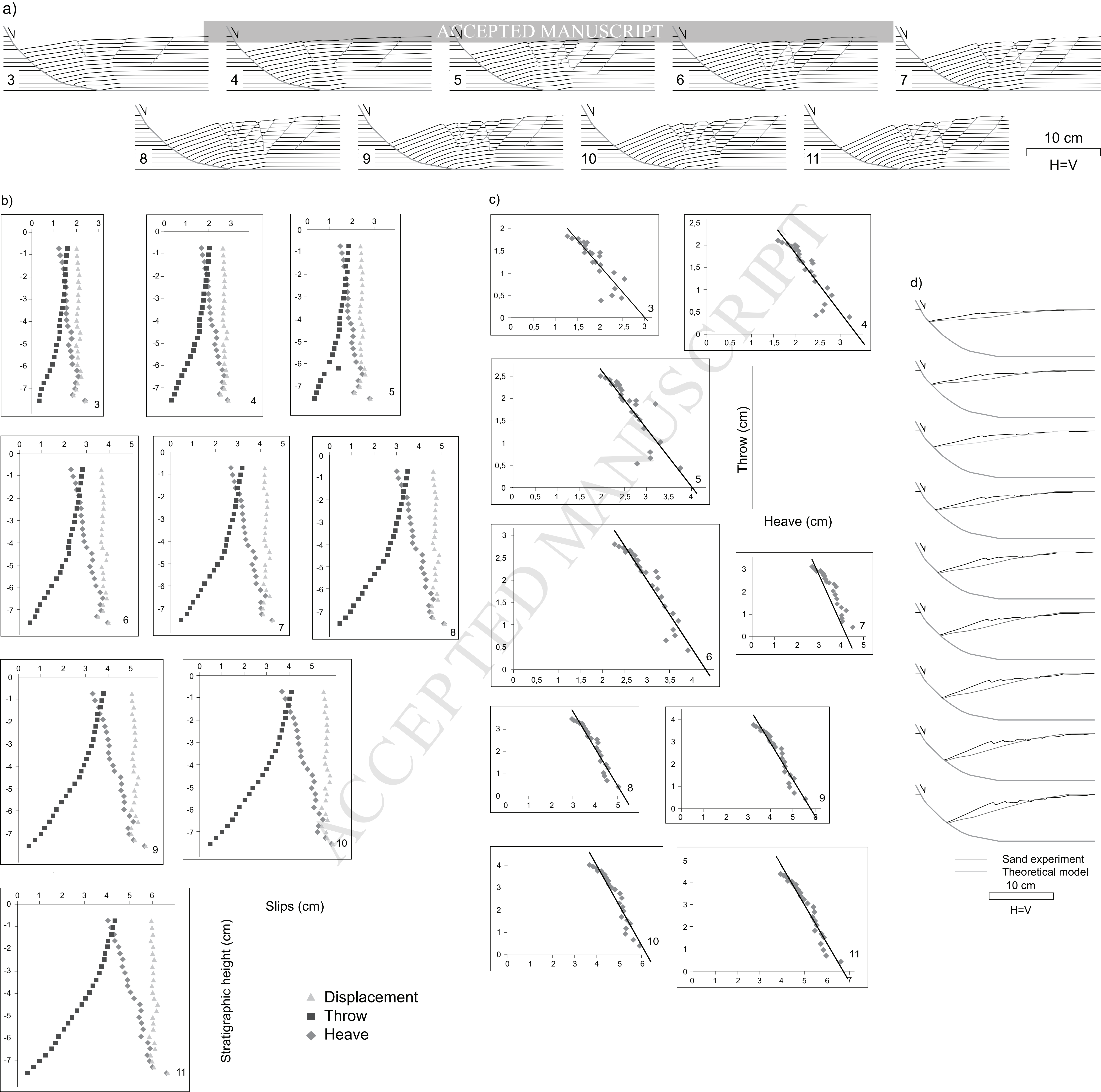
a)
10 cm
H=V
b)
c)
d)
Throw (cm)
Heave (cm)
Slips (cm)
Stratigraphic height (cm)
Displacement
Throw
Heave
Sand experiment
Theoretical model
10 cm
H=V

a)

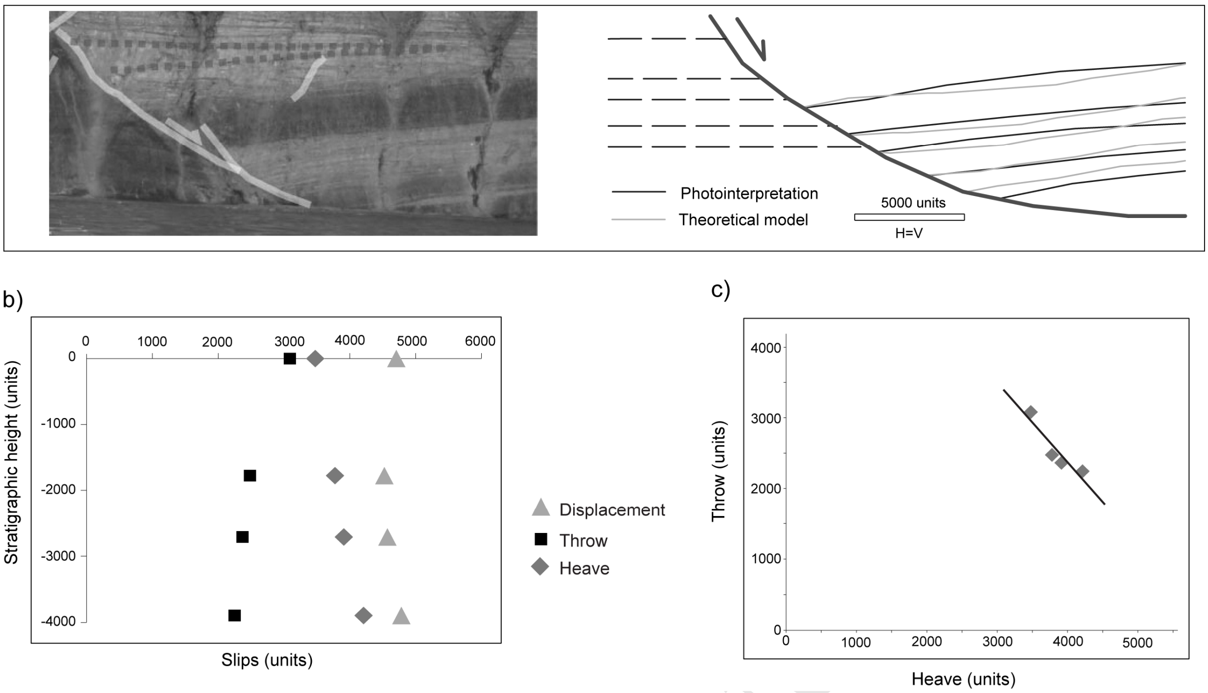
Photointerpretation
Theoretical model
5000 units
H=V
b)
Stratigraphic height (units)
Slips (units)
Displacement
Throw
Heave
c)
Throw (units)
Heave (units)

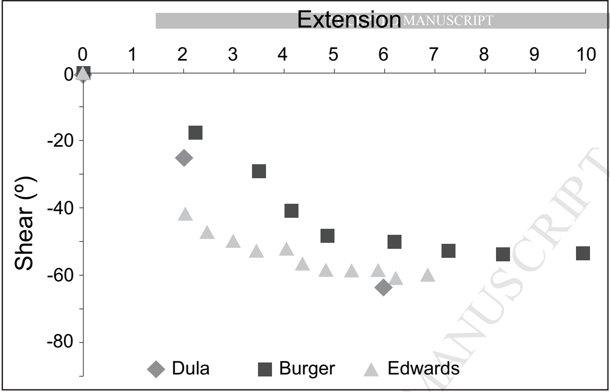
Extension
0
1
2
3
4
5
6
7
8
9
10
0
-20
-40
-60
-80
Shear (°)
Dula
Burger
Edwards

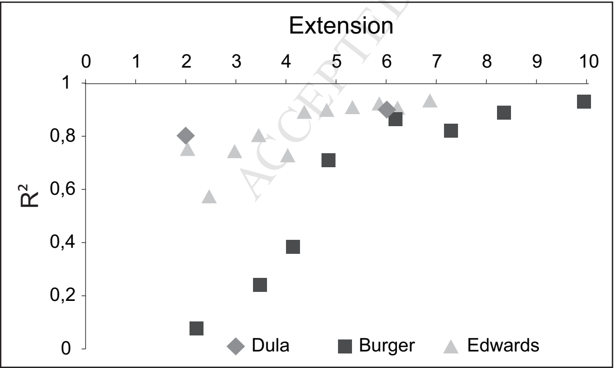
Extension
0
1
2
3
4
5
6
7
8
9
10
1
0,8
0,6
0,4
0,2
0
R²
Dula
Burger
Edwards

HIGHLIGHTS

-A method to estimate shear character and dip and amount of extension is proposed.

-It helps when reconstructing listric normal faults and associated structures.

-The effects of tectonic inversion and syntectonic sedimentation are considered.